February 2018

Master of Dissertation

Preparation and Characterization of Electrospun Lignin Carbon Fibers for Capacitive Deionization

축전식 이온제거를 위한 전기방사 리그닌 카본파이버 제조 및 특성화

Graduate School of Chosun University

Department of Chemical Engineering

Yong-Min Song

Preparation and Characterization of Electrospun Lignin Carbon Fibers for Capacitive Deionization

축전식 이온제거를 위한 전기방사 리그닌 카본파이버 제조 및 특성화

February 23, 2018

Graduate School of Chosun University

Department of Chemical Engineering

Yong-Min Song

Preparation and Characterization of Electrospun Lignin Carbon Fibers for Capacitive Deionization

Supervised by Professor Jae-Wook Lee

This dissertation is submitted to the Graduate School of Chosun University in partial fulfillment of the requirements for the Degree of Master in Engineering

October 2018

Graduate School of Chosun University

Department of Chemical Engineering

Yong-Min Song

Yong-Min Song's dissertation is certified

Thesis Committee Members

Ph.D./Prof. Jung-Heon Lee (Signature)
Committee chair

Ph.D./Prof. Hyun-Jae Shin (Signature)
Committee

Ph.D./Prof. Jae-Wook Lee (Signature)
Committee

November 2018

Graduate School of Chosun University

CONTENTS

LIST OF TABLES

LIST OF FIGURES

국문 초록

축전식 이온제거를 위한 전기방사 리그닌 카본파이버 제조 및 특성화

송 용 민
지도교수 : 이재욱
화학공학과
조선대학교 대학원

거대억새를 이용하여 바이오에탄올 제조하기 위한 공정에서 리그닌 제거를 위한 알카리 전처리 공정은 필수적이다. 이 과정에서 배출되는 리그닌 흑액으로부터 리그닌 회수 또는 폐수처리를 위해 본 학위논문에서는 순수한 리그닌 시약과 나노섬유 유도체인 PVA를 알카리 조건에서 혼합용액을 제조하였다. 제조된 혼합용액을 전기방사법을 통해 카본 파이버를 제조한 후, 안정화 및 탄화공정을 통해 확보한 카본파이버를 축전식 이온제거에 적용하였다. FE-SEM 표면분석을 통해 확인한 결과 매우 균일한 섬유 직경크기 분포를 갖는 나노파이버를 얻을 수 있었다. 또한 서로 다른 pH (8.0, 9.0)에서 제조된 리그닌/PVA 혼합용액으로부터 제조한 카본파이버의 비표면적은 1099~2133 m^2/g 범위에 있었다. 제조된 리그닌 카본파이버를 전극소재 및 축전식 이온제거용 카본전극으로 활용하기 위해서는 전기적 특성 파악이 매우 중요하다. 별도의 바인더 및 도전재를 사용하지 않고 제조한 카본전극에 대해 cyclic voltammetry를 통해 5 mV/s 주사속도 조건에서 측정한 결과, 리그닌 파이버 (pH 8, pH 9)의 축전용량은 각각 117 F/g, 143 F/g 였다. 100 mg/L 의 염화나트륨 수용액을 1.2V의 전압을 인가하여 측정한 결과, 리그닌 카본파이버 (pH 8, pH 9)의 탈염효율은 77.2%, 85.4%의 효율을 보였다.

Chapter 1. Introduction

1.1 Water shortage

The 21st century is bringing new challenges with population expansion, a decrease in natural resources, and climate change. Mean temperatures increased by 0.8℃ since 1880, with two thirds of the change occurring since 1975, and they are projected to increase by 3℃ to 4℃ by the end of the 21st century [1]. Temperature extremes have also increased by 75% because of climate change [2]. Continued population growth and to a lesser extent, climate change have also resulted in decreasing water resources [3,4]. As this water shortage problem accelerated, the water shortage problem in Korea Population Action International (PAI) has classified Korea into water scarcity country using Falk enmark indicator, Korea community have believed in “water scarcity” with no doubt. The output from PAI is consistent with that from report (2006) by the Korea ministry of Land, Infrastructure, and Transport (MOLIT) [5]. MOLIT also used the Falkenmark indicator, resulting in Korea as water scarcity country with available annual renewable water resources per capita of 1512 m^3. To solve this problem, seawater desalination technology is developed. World water resources are mainly salty (97.5%) and fresh water (2.5%). Salty water is found in oceans, seas and some lakes while fresh water is either stored underground (30%) or in the form of ice/snow covering mountainous regions, Antarctic and Arctic (70%) but only 0.3% is accessible by humans (Bigas,2013). With this limited amount of usable fresh water, desalination proposes the means to meet the increasing demand for fresh water [6]. Desalination of salty water is the separation of dissolved salts to produce fresh water with an allowed level of dissolved solids.

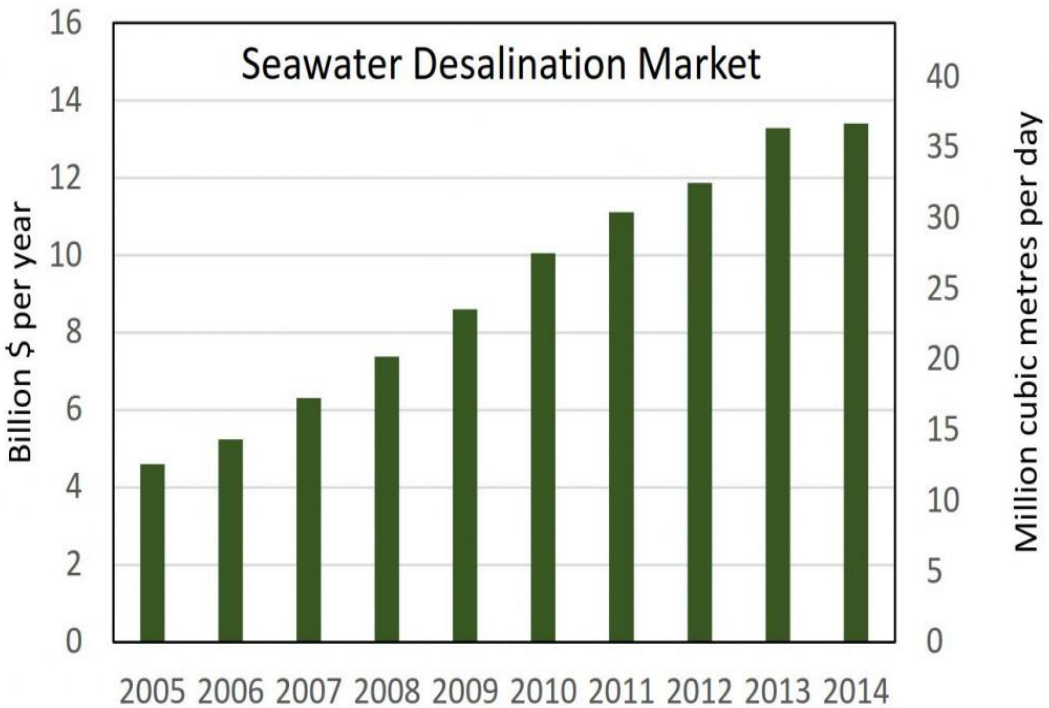

Figure 1.1. Growth of sewater desalination market [7]

1.2 Desalination technologies

1.2.1 Evaporation

The evaporation technology is a natural water circulation phenomenon occurring on the earth, that is, the steam is condensed in the low temperature atmosphere in the upper troposphere and it is cloudy, and then it drops to the surface or sea surface in rain form. When the sea water is evaporated, the solvent water evaporates, and the salt, the solute, separates the fresh water from the seawater by using the remaining property. It has the advantages of large capacity and high purity of production, but it has a disadvantage of high energy consumption Depending on the evaporation method and the steam recycling method, the Multi-stage Flash (MSF) method distillation, Multi Effect Distillation (MED), Vapor Compression Distillation (VCD) [8,9]. The MSF method is currently the most widely used desalination technology for large-capacity desalination plants, accounting for about 60% of the global desalination capacity. When the liquid at a temperature is suddenly reduced to a saturated vapor pressure corresponding to the temperature. It is consuming as latent heat of evaporation and self-evaporation or flash evaporation occurs [9].The multiple effect distillation method is a simple arrangement of a series of distillers in the first evaporator, When steam is heated to evaporate seawater, the resulting steam is condensed in an evaporator of the following utility. It becomes fresh water and acts as a heating source to evaporate seawater inside the evaporator. Also, The steam again acts as a heating source in the evaporator of the next utility [10].

1.2.2 Reverse osmosis (RO)

Reverse osmosis is a pressure driven separation technique. By applying a pressure difference, the permeating component, in most applications nearly exclusively water, are forced through the membrane. Besides its application for production of drinking water, reverse osmosis is also applied in the treatment of effluent water and separation of organic and inorganic compounds from aqueous solution for industrial applications [11,12]. The heart of RO based separation is the semi permeable membrane known as RO membrane which preferentially allows water molecules to pass through it, by obstructing the passage of salts under the influence of externally applied pressure (Figure 1.2.) [13]. The salt and water permeate through an RO membrane by solution-diffusion transport mechanism [14,15]. When the applied pressure is higher than the osmotic pressure ($\Delta p > \Delta \pi$), water starts flowing from concentrated salt solution to dilute solution through the membrane.

$$J = A(\Delta p - \Delta \pi) \qquad \text{Equation 1}$$

where $\Delta \pi$ is the osmotic pressure difference between the feed and the permeate, Δp is the pressure difference across the membrane and A is a constant which describe the physical characteristics of the membrane itself. RO membranes are characterized by the average pore size of less than 1 nm and require very high pressures up to 80 bar. Such high pressures are required to overcome the osmotic pressure of sea water, which is about 25 bar. The performance of these membranes is usually governed by water flux and salt rejection. An ideal RO membrane has a salt rejection of more than 99%. NF membranes are also used for desalination application, but the salt removal capacity is not as high as that of RO membrane. Depending upon the requirement or application of pure water, either NF or RO membrane can be used [13].

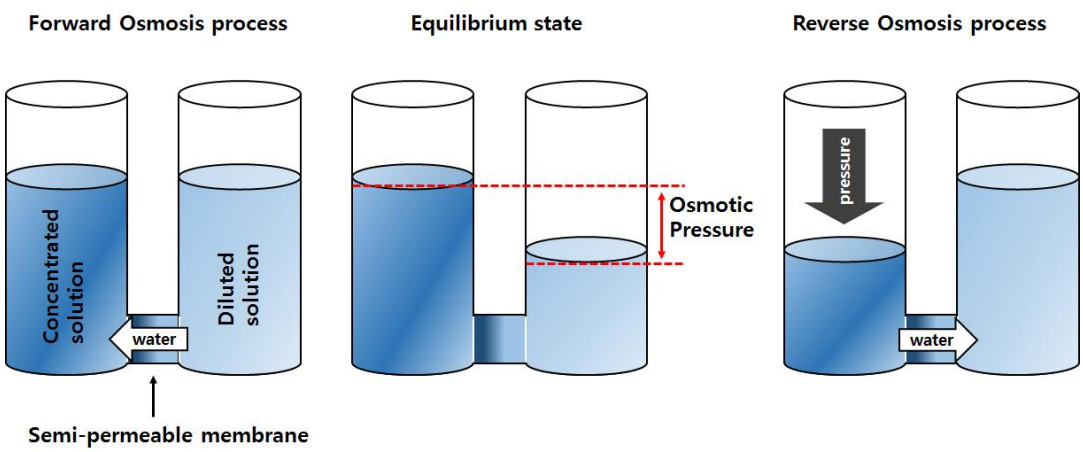

Figure 1.2. Principle of osmosis and reverse osmosis (RO)

1.2.3 Electrodialysis (ED)

Electrodialysis (ED) is a type of technology which arranges ion-exchange membranes alternately in a direct current field. There are five elements complementary for ED applications [16]. (1) electrodes, where the oxidation and reduction reactions occur to realize the transformation from ionic conduction to electron conduction and thus supply the original driving force for ion migration; (2) direct current supply, which proves effective to reinforce ion migration; (3) solvents, which make a continuum for ion transport by filling the space between electrodes and membranes; (4) ion exchange membranes, the key points which permit the transport of counter ions and block the passage of co-ions; (5) electrolytes, the current carriers between cathode and anode. ED has been widely used to demineralize, concentrate and convert salt-containing solutions [16-18]. however, ED is not so economically competitive as other membrane separations, such as ultrafiltration (UF) ,reverse osmosis (RO), and microfiltration (MF) [18]. The main reasons are the high cost of ion exchange membranes and electrodes and short life time of membranes when working in high-density electrical field [18].

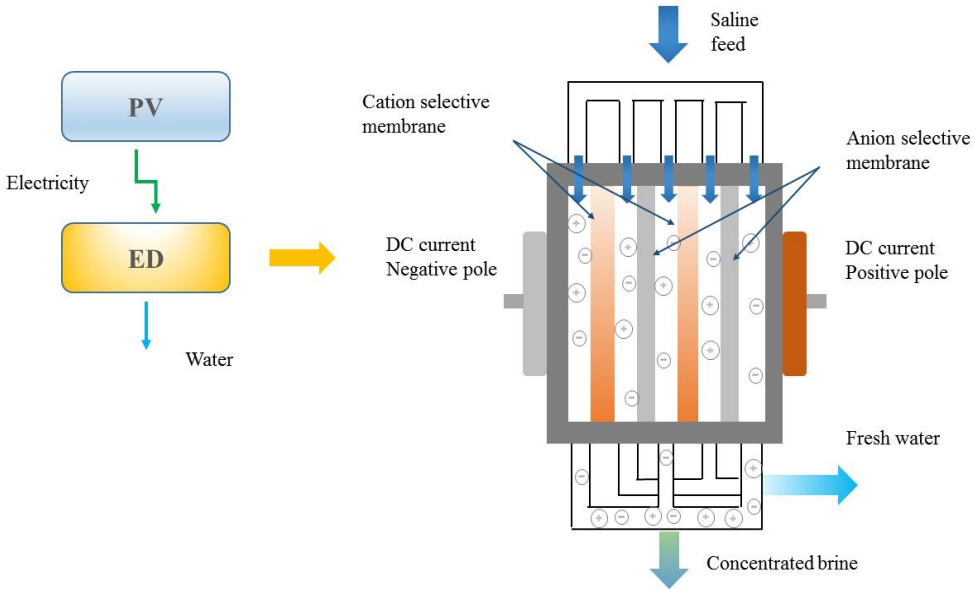

Figure 1.3. Principle of electrodialysis (ED)

1.2.4 Ion-exchange

IE is a fixed-bed separation technology using ion exchange resins [19]. These resins have a large number of tightly attached bonds on their surfaces, which can reversibly absorb one type of ions. The physical form of the resins is a small sphere with a diameter between 0.4 and 0.8 mm. A cation exchange resin captures positively charged ions and an anion exchange resin negatively charged ions. In fresh resin, the cations attached to the cationic resin are H^+, those attached to the anionic resin OH^-. Passing raw whey over a bed of cation exchange resin would result in exchange of the cations in the whey against H^+ ions. Subsequent passage of this whey through the anion exchange resin would absorb anions, displacing the OH^- ions. As a result, desalted whey exits the anion exchange resin column. The capacity of exchangeable ions is limited [20]. The amount of whey that can be desalted by the given quantities of resins can be calculated. The same applies to the required amount of water and regenerants (acid in the case of cation exchange resin, alkali in the case of anion exchange resin). These solutions are sufficiently concentrated to remove the absorbed cations and anions and replace them by H^+ and OH^- ions, regenerating the resins to their previous state.

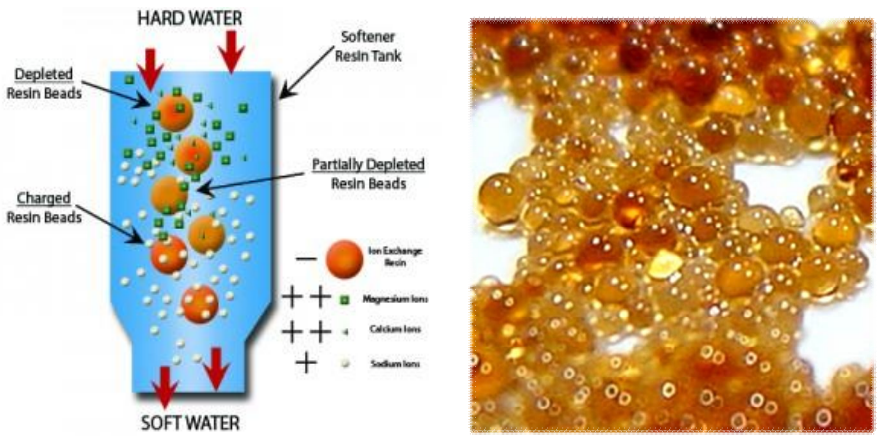

Figure 1.4. Principle of ion-exchange [21]

1.2.5 Capacitive deionization (CDI)

CDI is a method for removing dissolved salts from brackish water by their adsorption onto electrode surfaces to form electric double-layers (EDL), and now is a potential method for desalination of drinking water. Since the adsorption mechanism of CDI is the same as that of electric double-layer capacitors for energy storage. electric double-layers is a basic concept in electrochemistry [22]. When the electrode is charged and put into a solution with ions, the interface of the charged electrode and ions abundant solution will be filled with counter ions as a result of the Coulomb force, forming EDL [26]. Reducing the charge hence the removal of Coulomb force releases the held ions back to the solution. This taking up and release can be used as deionization and regeneration in desalination [26]. The first model for CDI based on electrical double layer was developed by Johnson and Newman in the 1970s [23,24]. First model was assumed that ion sorption in the CDI is approximated as capacitive process; kinetics of adsorption does not limit the rate and faradaic reactions are negligible. The model has been widely used to investigate the process and explain experimental results. Interfacial properties and structures between an electronic conductor (electrode) and an aqueous electrolyte solution have been explained well by widely accepted Gouy-Chapman-Stern double layer theory [25]. According to the Gouy-Chapman-Stern model, the double layer can be assumed to be divided into an inner area and a diffusion area [26]. The inner area is named as the Helmholtz layer where ions covered directly onto the surface of electrode, while the area further from the surface is a diffusion layer called the Gouy–Chapman layer where the distribution of electric charge is depended on the potential at the surface [26]. Both capacitances of the two layers contribute to the total capacitance; thus, the total capacitance can be calculated like a series union of both the inner Helmholtz layer and diffuse Gouy–Chapman layer The following advantages of CDI have been mentioned: no chemicals are required during the cycles of desalination and regeneration, and the applied voltages are fairly low to avoid the electrolysis of water, which make this technology nonpolluting, environment-friendly, energy efficient and cost-effective for water desalination.

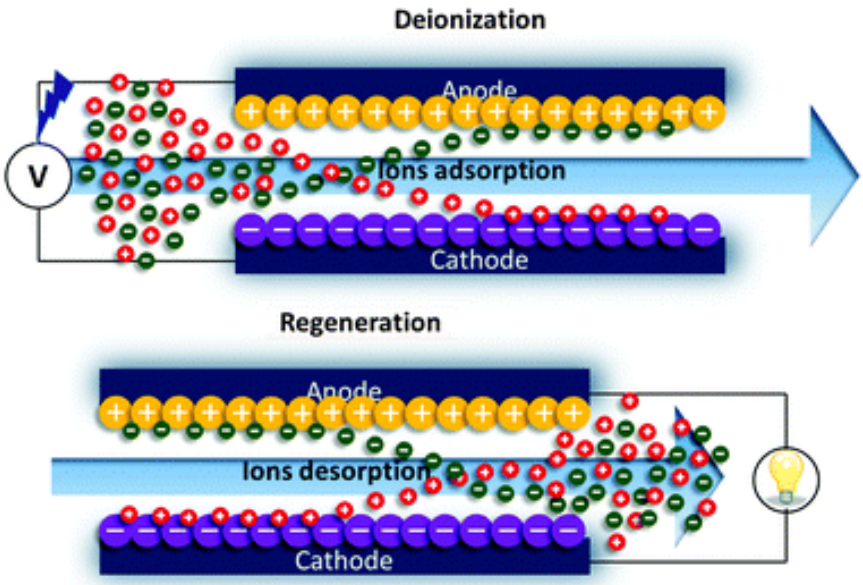

Figure 1.5. Desalination principle of capacitive deionization [27]

Table 1.1. Energy comparison of desalination technology [28]

Desalination technology	Evaporation	MFE	ED	RO	CDI
Basic mechanism	Steam is salt-free condenses to Form pure water	Steam is salt-free condenses to Form pure water	Ions move through anions and cation membrane	Ions move through anions and cation membrane	Ions adsorb and/desorb on electrode due to DC voltage
Total capital Cost	High	High	Medium-high	Low	Low
Energy requirement	6.6 kWh/m^3 (~ 125 Wh/gal)-seawater	7.9-10.8 kWh/m^3 (30-41 Wh/gal)-seawater	2.03 kWh/m^3 (7.7 Wh/gal)-brackish water	6.6-9.3 kWh/m^3 (25-35 Wh/gal)-seawater	~4.2-8.5 kWh/m^3 (16-32Wh/gal)-seawater 0.05-0.1 kWh/m^3 (0.2-0.4 Wh/gal)-brackish water
Challenge analysis	Better scale control materials hybrid optimization	Better scale control materials	Lower cost, Membranes And ED optimization	Better membranes and module design; high-performance membrane from nanotechnology	Practical modules and scale-up; novel nano structures electrodes with high energy recovery

Chapter 2. Literature review of CDI

2.1 Capacitive deionization (CDI)

2.1.1 Electric double layer (EDL)

Electrical double layer theories. In Figure 2.1. schematically shows different electrical double layer (EDL) models proposed over time. The concept of EDL was first introduced by Helmholtz who suggested that a charged surface immersed in an electrolyte solution repels ions of the same charge (positive or negative) but attracts their counter-ions [29]. The layer of electronic charge at the electrode surface and the layer of counter-ions in the electrolyte forms what has been termed the electrical double layer [30,31]. The Helmholtz model hypothesized that counter-ions form a monolayer near the electrode surface, as illustrated in Figure 2.1a. [29]. This structure is analogous to that of conventional dielectric capacitors with two planar electrodes separated by a small distance H, approximated as the radius of anion [29-31]. The Helmholtz model was modified by Gouy [32] and Chapman [33] with the consideration that the ion distribution should be continuous in the electrolyte solution and given by the Boltzmann distribution. The Gouy-Chapman model accounts for the fact that the ions are mobile in the electrolyte solution under the combined effects of ion diffusion driven by concentration gradients and electromigration driven by the electric potential gradient, i.e., the electric field. This results in the so-called “diffuse layer” illustrated in Figure 2.1b. However, the Gouy-Chapman model overestimates the electrical double layer capacitance because it treats ions as point-charges resulting in unrealistically large ion concentrations at the electrode surfaces [30,31,34]. In 1924, Stern proposed a new EDL model accounting for the finite size of ions. Stern [35] combined the Helmholtz model and the Gouy-Chapman model to explicitly describe two distinct regions, namely (1) the inner region of thickness H termed the Stern layer and (2) the outer region called the diffuse layer, as shown in Figure 2.1c. In the diffuse layer, the ions are mobile under the

coupled influence of diffusion and electrostatic forces, and the Gouy-Chapman model applies in this layer [36]. [30-32] In 1947, Grahame [38] improved this model by eliminating a number of deficiencies. The author emphasized that in the Stern layer, specific (covalent) and non-specific adsorption of ions at the same electrode surface lead to different closest distances from the charged surface [31,32,35,37]. The inner Helmholtz plane (IHP) consists of ions adsorbed by specific (covalent) forces and the outer Helmholtz plane (OHP), or Stern layer, of ion adsorbed by non-specific (electrostatic) forces. However, continuum models of EDLCs typically consider only electrostatic adsorption, corresponding to the Stern model. Note that electroneutrality does not prevail within the electrical double layer

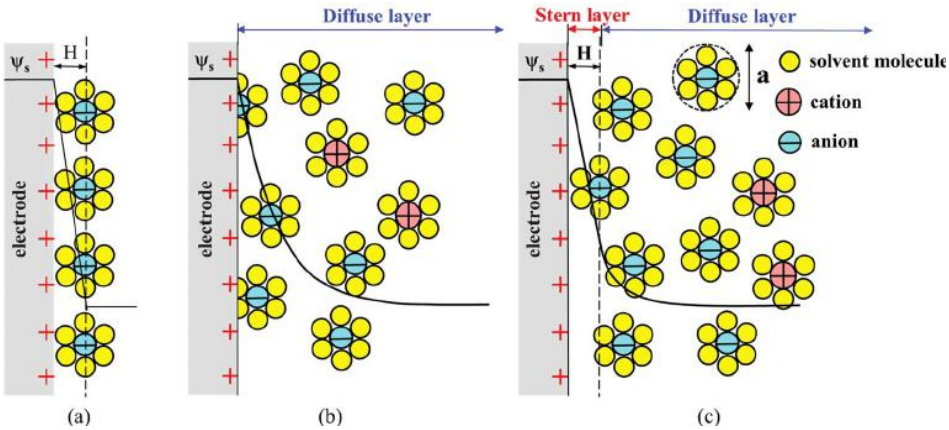

Figure 2.1. Schematic representation of electrical double layer structures according to (a) the Helmholtz model, (b) the Gouy-Chapman model, and (c) the Gouy Chapman-Stern model. The double layer distance in the Helmholtz model and the Stern layer thickness are denoted by H while ψ s is the potential at the electrode surface [39]

2.1.2 Faradaic and non-faradaic reaction

Electrochemical currents can be classified into two types: Non-Faraday currents due to the accumulation of faraday current and charge due to the direct transfer of electrons / charges. The faraday current consists of the transfer of electrons by the oxidation-reduction reaction on the electrode surface, and the transfer of the redox reaction material in the electrolyte solution. On the other hand, a non-Faraday current is formed when a substance (ion or molecule, etc.) having charge on the interface is simply collected regardless of the electrochemical reaction. The most representative example is the electric double layer. When a voltage is applied to the electrode, the electrode becomes polarity (+) or (-). In the solution, materials having opposite charges are induced by the electrostatic attracting force and accumulate at the interface to form two layers having different charges. In addition, adsorption of charged materials also forms a non-Faraday current

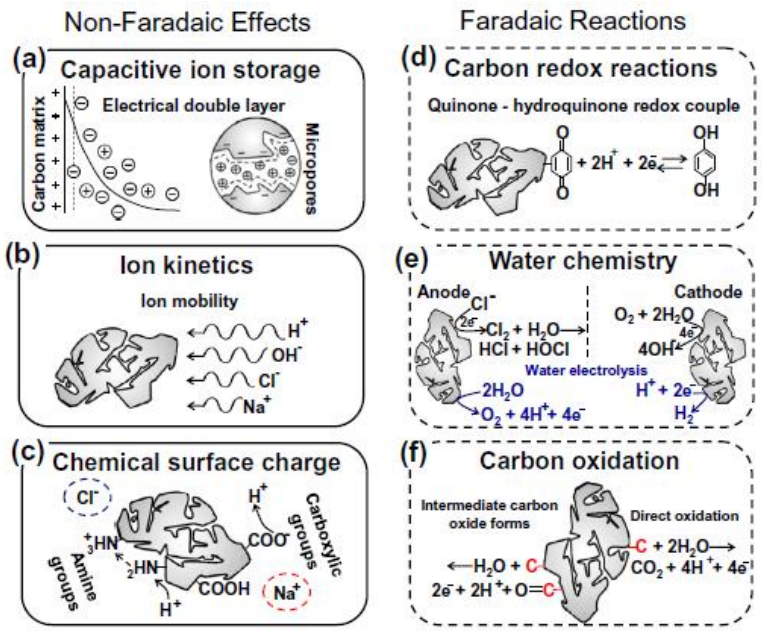

Figure 2.2. Overview of important electrochemical reactions and processes in CDI electrodes. Effects (a–c) can be classified as non-faradaic, and (d–f) as faradaic processes [22]

2.1.3 Membrane capacitive deionization (MCDI)

During the charging process in CDI, ideally the cations alone should move into the porous cathode material and anions alone should move into the positively charged anode material. During the discharge process, these ions should move out [22]. However, in real experiments, the coions will also move into the anode and cathode surfaces. This would lead to loss of efficiency of deionization. To overcome this problem, ion-selective membranes are fixed closer to the electrode surface. Cation exchange membrane near the cathode will allow cations to selectively move in (charging) and out (discharging). Anion exchange membrane will function similarly near the anode allowing selective anion movement [26]. This modification is termed as membrane capacitive deionization (MCDI) shown in Figure 2.3.. The salt removal efficiency of MCDI cell was enhanced by 32.8−55.9 % compared to CDI cell, and current efficiency of 83.9−91.3 % was higher for the MCDI compared to 35.5−43.1 % for the CDI [40]. Conceptually, MCDI is certainly an improvement over CDI. However, the ion exchange membranes certainly may increase the cost of production of CDI unit. During the past few years, selective coating of carbon electrodes with ion exchange resins is found to be an effective alternative approach than using separate membranese

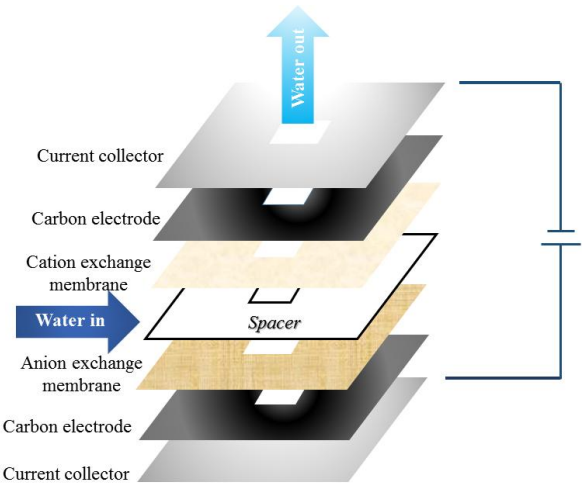

Figure 2.3. Schematic diagram of MCDI cell and desalination system

2.2 Carbon electrode

2.2.1 Activated carbon (AC)

AC has been the mostly used electrode materials in CDI mainly because its low cost. It was actually the first electrode materials used for electrosorption [26]. The variety of precursor materials and synthesis conditions translates to an equally great variety in pore structures and surface chemistry of the resulting AC material. Thus, a detailed description of the properties, the pore structure, is important for any comprehensive understanding and comparison of the desalination capacity of AC electrodes [41]. As a general trend, an increase in the specific surface area and total pore volume results in a higher salt adsorption capacity [22].

2.2.2 Carbon nanotube (CNT)

Carbon nanotube (CNT) is novel carbon materials with unique structure and extraordinary electrical properties. A single-walled carbon nanotube is a rolled graphene sheet in a cylindrical shape. A tube surrounding tube structure made of two layers of graphene sheets is called double-walled carbon nanotube and the one made of more than two layers of graphene sheets is called multi-walled carbon nanotube [26] .Depending on the arrangement of the hexagon rings along the tubular surface, CNT can be metallic or semiconducting.

2.2.3 Carbon aerogel

Carbon aerogels are carbon particles in the form of aerogels, pores are interconnected, and pore size and density are easily controlled. It has high specific surface area, low electrical resistance, nano-sized porous structure, and excellent electrical conductivity, making it an ideal electrode material for CDI. When carbon aerogels are applied to CDI technology, they have 10 ~ 20 times more energy efficiency than conventional processes, and they can contribute to simplification of processes and prevention of pollution because

they do not require the use of high pressure pump or membrane.

2.2.4 Activated carbon fiber (ACF)

Activated carbon fiber is a material that has been developed to enhance the adsorption power of activated carbon, and refers to carbon in fiber form. The activated carbon fibers have a narrow and uniform pore size distribution and have a larger specific surface area than the activated carbon. It has high electrical conductivity and heat resistance and high elasticity. However, the activated carbon fiber has disadvantages such as complicated manufacturing process and high production cost.

2.2.5 Biomass-derived carbon

The biomass resources are abundant, including energy crops, agricultural crops and their residues, wood and wood wastes, municipal wastes and animal wastes, aquatic plants and algae. Biochar and ACs are the most common products from biomass materials. Briefly, biochar usually can be obtained by burning or pyrolysis (low oxygen) of biomass materials, which often produced highly porous structure with a high specific surface area. ACs are another kind of by-products that can be obtained from the pyrolysis of biomass materials, usually possessing high specific surface area and rich porosity, which have been widely used for gas separation, water purification, catalyst supports, electrodes for supercapacitor and fuel cells

Table 2.1. Summary of biomass-derived carbon electrodes for SCs through pyrolysis and/or activation [42]

Materials	Activation agent	Activation temperature and time (℃)/(h)	SSA (m^2 g^{-1})	C (F g^{-1})	Measurements at	Electrolyte
Eggplant	N/A	N/A	950	121	5 mV s^{-1}	6 M KOH
Corncob	Steam	850/0.75	1210	120	1 A g^{-1}	6 M KOH
Coffee beans	$ZnCl_2$	900/1	1021	134	0.05 A g^{-1}	1 M $TEABF_4$/AN
Chestnut shell	$ZnCl_2$	800/1.5	1987	92	10 A g^{-1}	6 M KOH
Cotton stalk	H_3PO_4	800/2	1481	114	0.5 A g^{-1}	1 M $TEABF_4$/AN
Rice husk	Microwave-assisted $ZnCl_2$	600 W/1/3	1552	94	0.05 A g^{-1}	1 M Et_4NBF_4/PC
Bagasse pitch	Microwave-assisted $ZnCl_2$	700 W/0.25	-	138	0.2 A g^{-1}	1 M $EMIMBF_4$

2.3 Principle of electrospinning

Electrospinning is a method of realizing continuous fibers with a diameter of - μm to - nm by using an electric field. It is simpler than conventional self-assembly, phase separation and template synthesis, And has attracted much interest in biomedical / industrial applications based on various properties due to the high specific surface area due to the shape, porosity and ease of structure / size control. The electrospinning device consists of three kinds of high voltage, spinning protrusion and dust collecting plate collecting fibers as shown in Figure .2.4. The polymer solution is discharged at a constant rate through a pump, through a nozzle serving as a spinneret. In this case, one electrode connects the power supply with the nozzle tip, injects charge into the polymer solution to be discharged, and connects the opposite electrode to the dust collecting plate. When a high voltage of 0 to 30 kV is applied to the nozzle tip, the following two (1) mutual electrostatic repulsion between the surface charge and (2) the external electric field The polymer droplets of the liquid phase are drawn in the form of a funnel-shaped funnel by the applied Coulomb force. When an electric field of a specific intensity is applied to the nozzle tip in contact with the polymer solution, one side charge of + or - is accumulated in the polymer solution and the hemispherical shape of the tip of the nozzle exceeds the surface tension of the polymer solution due to mutual repulsive force of the same charge.

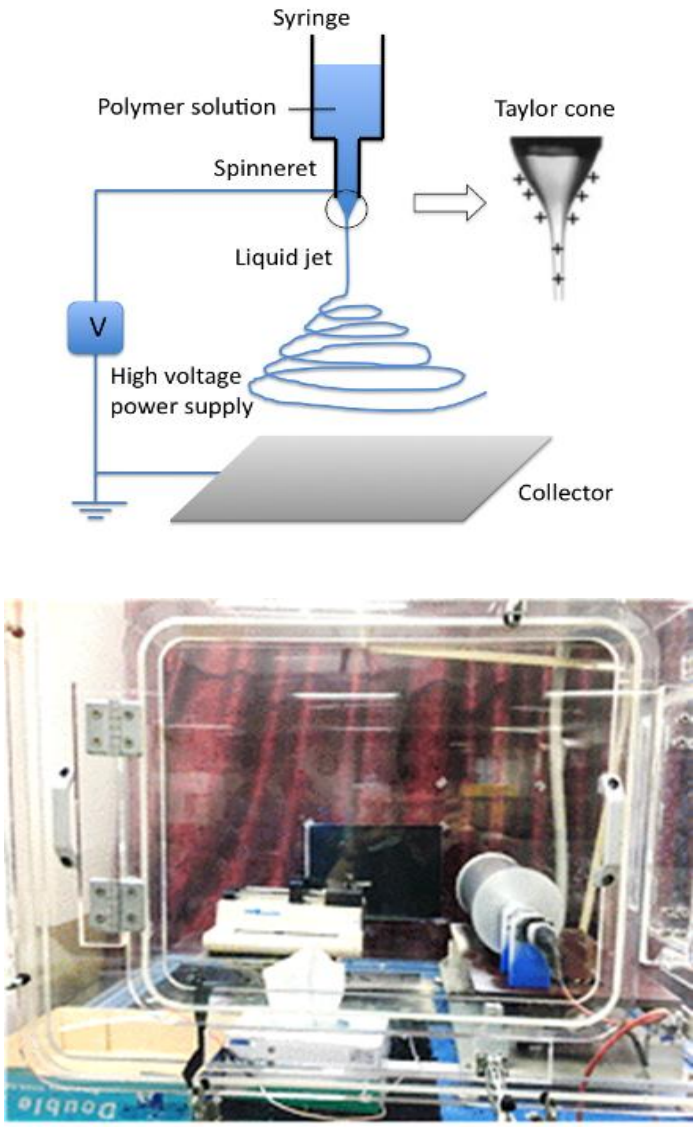

Figure 2.4. Schematic of Electrospinning setup

2.4 Trend of research

There are three major research trends in CDI research. The first is the study of the new system, the second is the separation purification of the substance and the contaminant removal. The third is the study of the carbon electrode, which is the most actively studied in the CDI composition, On the system flow capacitive deionization (FCDI) has been studied. The flow-electrode, which is a 5 mass% suspension of AC granules in a 0.1 M aqueous solution of NaCl, replaces the fixed carbon electrodes of the conventional CDI and flows through a channel carved on the current collectors. This system has some advantages, as a continuous desalination process and a high removal efficiency from salt water with high concentration, such as seawater, because the flow-electrode has infinite ion adsorption capacity, in contrast to a limited electrosorption capacity of the fixed electrode in CDI process [43-45]. In the separation purification section, a technique of desalinating a low concentration of seawater is generally studied, and recently, it is also used for removing impurities in the separation and purification process of a drug. In addition, as interest in rare metals increases worldwide, studies are under way to recover valuable metals. Finally, graphene has been studied in different forms, by using a binder as PTFE either with or without conductive material such as carbon black and graphite powder, as usual way to fabricate electrode sheets for supercapacitors, by using graphene foams, and by mixing with other active materials, such as metal oxides, AC and CNTs [46-48]. In recent years, CNT and CNF are mainly manufactured by CVD method, and CNF is often manufactured by electrospinning. CNF is mainly used as a PAN polymer which has environmental problems because it uses DMF as a solvent. Therefore, PVA polymer that water as a solvent was eco-friendly and non-toxic. In addition, electroactive materials mainly used in these polymers are required materials that can be easily obtained from nature.

2.5 Research objective

The lignin used in the bioethanol extraction process is used as an electroactive material having high added value [22,49]. Separation of cellulose and lignin through an alkali pretreatment, NaOH is generally used as a chemical activator, it is expected that it will be able to make high surface area carbon electrode without additional activation process because it is actually contained in lignin black liquor. However, since the exact components of lignin are not known, the present study has been conducted by adjusting the pH of the lignin reagent at the previous stage. Therefore, discarded lignin and non-toxic PVA were electrospun and then obtained lignin carbon fiber through stabilization carbonization process. The lignin carbon fiber was expected to be eco friendly and useful electrode materials having a high specific surface area. Finally, it is applied to CDI to evaluate desalination performance.

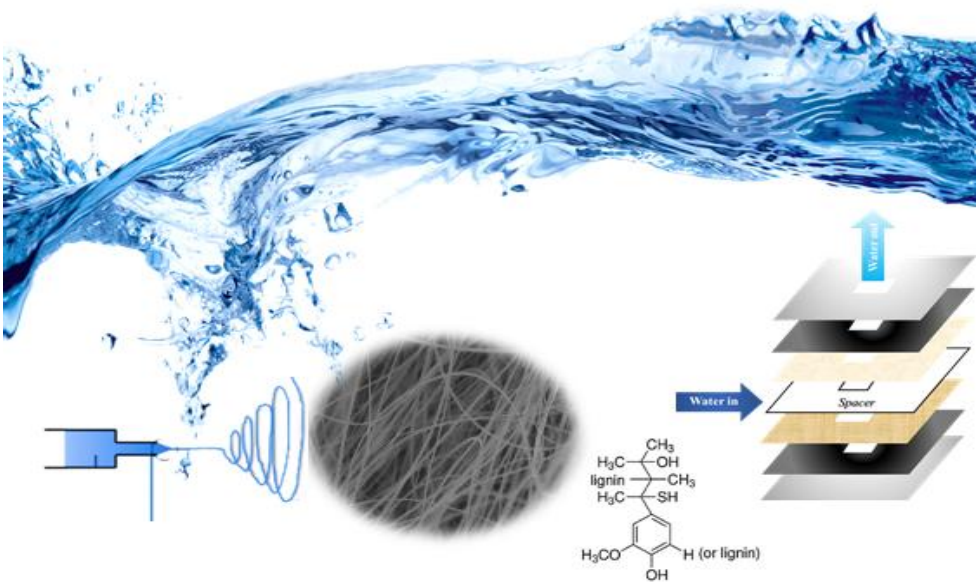

Figure 2.5. Overall schematic process of lignin carbon fibers

Chapter 3. Experimental

3.1 Fabrication of lignin carbon fibers

3.1.1 Properites of lignin

Lignin is a major component of the cell wall of a plant and plays an important role in making the structure of the tree which is main source of 22-29% (weight) after wood-based cellulose (40-43% weight). Lignin is a by-product of remnant after making cellulose into a major product in the pulp manufacturing process. In the pulp and paper industry, lignin was an unnecessary material that had to be removed to increase whiteness. Recently, lignin, a process by-product, is being produced in the process of producing bioethanol using woody biomass. The chemical structure of lignin undergoes a change during the process of removing lignin by pretreatment using enzymes and solvents to separate sugars of ethanol fermentation material from wood. In this study, kraft lignin low sulfonate (sigma-aldrich) was used to obtain lignin from black solution using sodium sulfide / sodium hydroxide solution, which is the most commonly used extraction method.

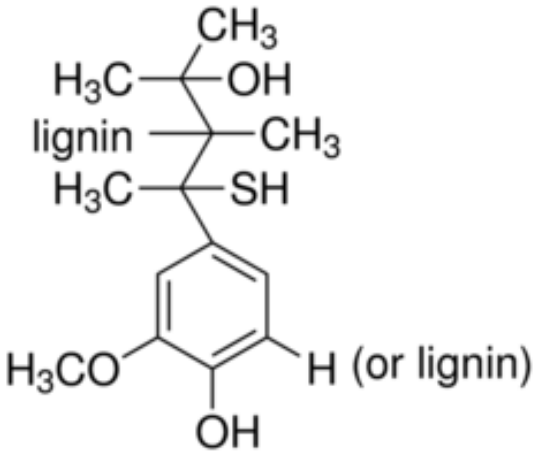

Figure 3.1. Structure of kraft lignin

3.1.2 Electrospinning of spinning solution

The spinning solution was prepared in two ways, assuming the lignin extracted from the actual waste solution. Lignin reagent solution, and NaOH solution. 15 wt%, 17.4 wt.%, And 23 wt.%, 28 wt% Respectively, in order to find the ratio of optimum lignin and PVA (20:80) (50:50) (75:25) respectively [50,51]. After stirring for about 6 hours at 80 ° C using a hot plate, lignin was added according to the ratio and the total amount of the polymer. After stirring for about 6 hours, the temperature was lowered to room temperature and stirred for about 12 hours. The spinning solution used was an electrospinning device, the voltage applied to the spinning was 15 kV, and the distance between the syringe and the collector was maintained at 15 cm. Syringes were used in a volume of 10 mL and the diameter of the injection needle was 0.5 cm. The flow rate of the solution was 1 ml/hr and the rotation speed of the collector was 100 rpm.

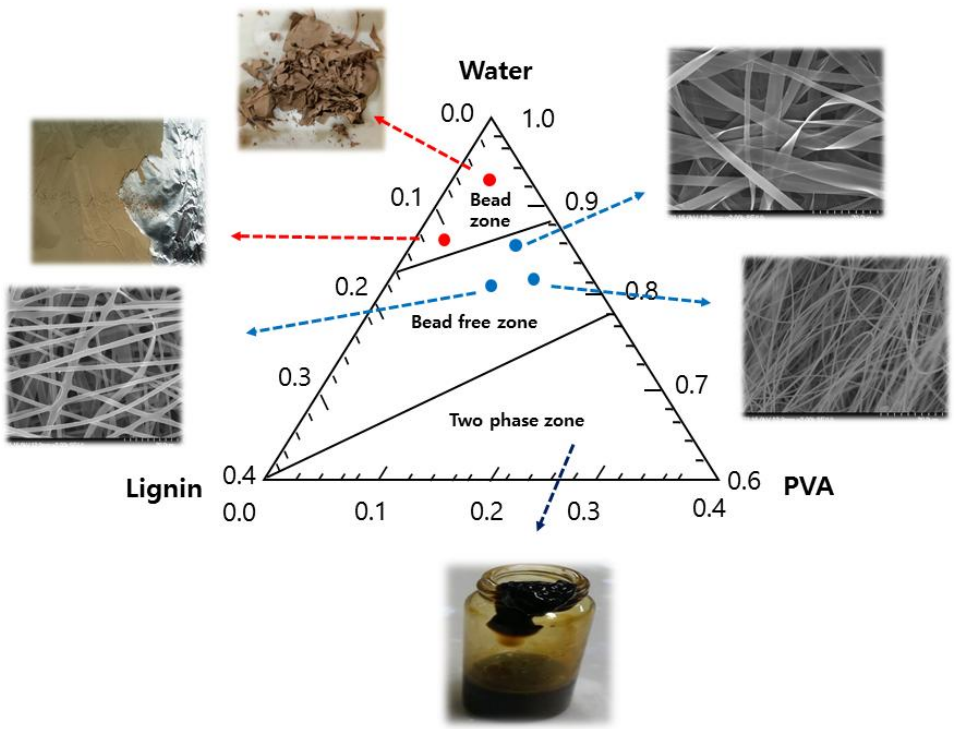

Figure 3.2. Ternary diagram indicating electrospinnability domains according to the composition of the precursor solutions (mass fractions of lignin, PVA, and water)

3.1.3 Stabilization and carbonization

As a starting material, PVA, which is a linear polymer, is stabilized at 200 to 300 ° C for 1 to 2 hours in the air, and the precursor material can withstand the carbonization process by chain cleavage, cross-linking, dehydrogenation and cyclization. A thermally stable ladder structure is obtained and the yield of carbonization is improved [52]. During the stabilization reaction, the shrinkage should be within 15% by stretching to maintain and improve the molecular orientation. During the stabilization process, a complex chemical reaction is accompanied by the release of H_2O, CO_2, HCN, etc., resulting in a weight loss of 5-8%, and the carbon content in the precursor fibers decreases from 68% to 62-65%. When this precursor material is carbonized in an inert atmosphere at 1200 to 2500°C, about 50% by weight of carbon fiber is obtained based on the precursor material. Since the carbon fiber is composed of only carbon, no further weight reduction occurs in the graphite process at 2500℃ or higher, and the crystal orientation of the carbon fiber in the fiber axis direction is increased Only the structural changes occur and the mechanical properties of the final carbon fiber are improved. However, in this study, the stabilization process using an electric furnace was carried out at 250℃ for 4 min. After cooling at room temperature, N_2 gas, which is an inert gas, was flowed at 400 ml/min using a tubular furnace. The temperature was raised to 2°C per minute up to 700°C, and then maintained for 2 hours.

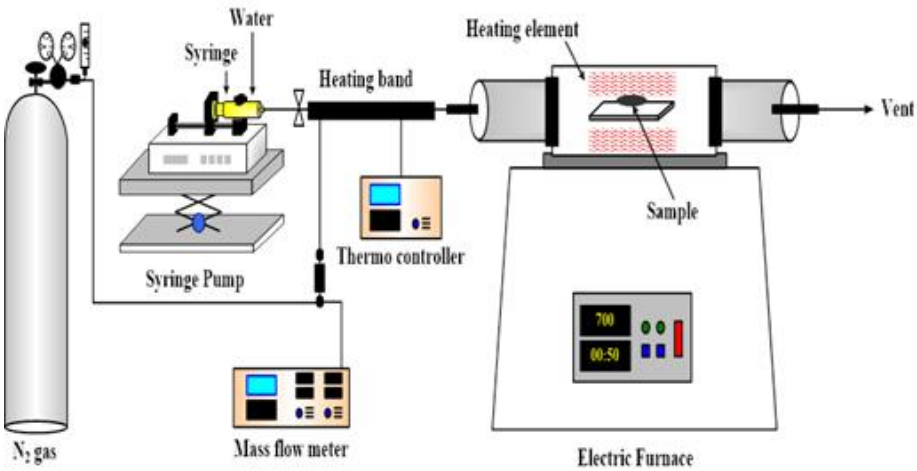

Figure 3.3. Schematic diagram of carbonization and activation apparatus.

3.2 Electrochemical properties

The carbon fibers were evaluated for small electrode without binder and current collector. The CHI 660e instrument was used for the electrochemical measurement, and cyclic voltammetry (CV), chronocoulometry (CC), chronoamperometry (CA), and AC Impedance were used to evaluate the adsorption and desorption characteristics of the carbon electrodes. Respectively. CV was measured by measuring the current flowing through the cell while changing the potential at the same rate in a constant electrode potential range. The capacitances of the activated carbon electrodes and the adsorption and desorption characteristics at the electrodes were analyzed. CA and CC analyze the adsorption rate and adsorption amount of ions on the carbon electrode by measuring the amount of electric current and charge flowing through the cell while maintaining the electrode potential at a constant level. The prepared carbon electrodes were fixed in the circular part that reacts to the kit shown in Figure 3.4. Then, 1 mL of 4 M NaCl as an electrolyte was filled, and then an Ag / AgCl reference electrode and a Pt counter electrode were placed, followed by electrochemical analysis. CV analysis was carried out with varying potential scanning speeds ranging from -0.6 V to 0.6 V at 5, 10 and 25 mV/s. The CA and CC analyzes were carried out by applying a constant potential of -0.6 V for 100 sec and immediately applying 0.6 V for 100 sec. The change of current and total charge over time was measured in adsorption and desorption reactions.

Figure 3.4. Electrochemical measurement cell kit for flexible carbon fiber

3.3 Evaluation of desalination performance

The evaluation of desalting performance, the unit cell was constructed and the CDI experiment was conducted. Two 1.5 cm thick acrylic plates of 10 x 10 cm^2 were prepared. One acrylic plate was drilled with a 1 cm diameter hole at the center and both diagonal ends to allow the solution to flow from both diagonal ends to the center. Two porous carbon electrodes of 6.5 x 6.5 cm^2 were prepared and holes were drilled at the center and both diagonal ends of the carbon electrode for positive electrode to secure the flow path of the influent. A CDI unit cell was constructed by inserting an anion exchange membrane on a carbon electrode for a positive electrode and a cation exchange membrane on a carbon electrode for a negative electrode and inserting a nylon sheet having a thickness of 90 μm between the two ion exchange membranes.

Figure 3.5. Automatic capacitive deionization test system

Chapter 4. Result and discussion

4.1 Characterization of lignin carbon fibers

4.1.1 Field emission scanning electron microscopy (FE-SEM)

The surface properties of lignin carbon fibers were confirmed by FE-SEM. Fiber -stabilization - carbonization, and the change of fiber was observed according to thermal properties. At 15 wt% and 17.4 wt% of total polymer, the fibers could not be laddered at the stabilization stage and could be broken. At 28 wt%, it was confirmed that the structure was broken due to the cohesion between the fibers due to the high viscosity. Therefore, the change of fiber diameter at 23wt% according to the thermal properties of two samples with pH8 and pH9 with NaOH could be confirmed. The average diameters of pH 8 samaples different conditions at fiber, stabilization and carbonization were 0.79 μm, 0.58 μm 0.37 μm, respectively (Figure 4.1. a-c). Lignin fiber (pH 8), it can be seen that the diameter decreases with stabilization and carbonization process. The reduction in diameter shows a general fiber stabilization and carbonization process. In contrast, the average diameters of lignin fiber (pH 9) samaples different conditions at fiber, stabilization and carbonization were 0.46 μm, 0.4 μm 0.34 μm, respectively (Figure .4.1 d-f). In Figure .4.2 shows that the diameter is smaller lignin fiber (pH 8) than lignin fiber (pH 9). It is considered that stronger elongation forces were imposed to the ejected jets under the electrical field due to an increased charge density in pH 9 solution [53].

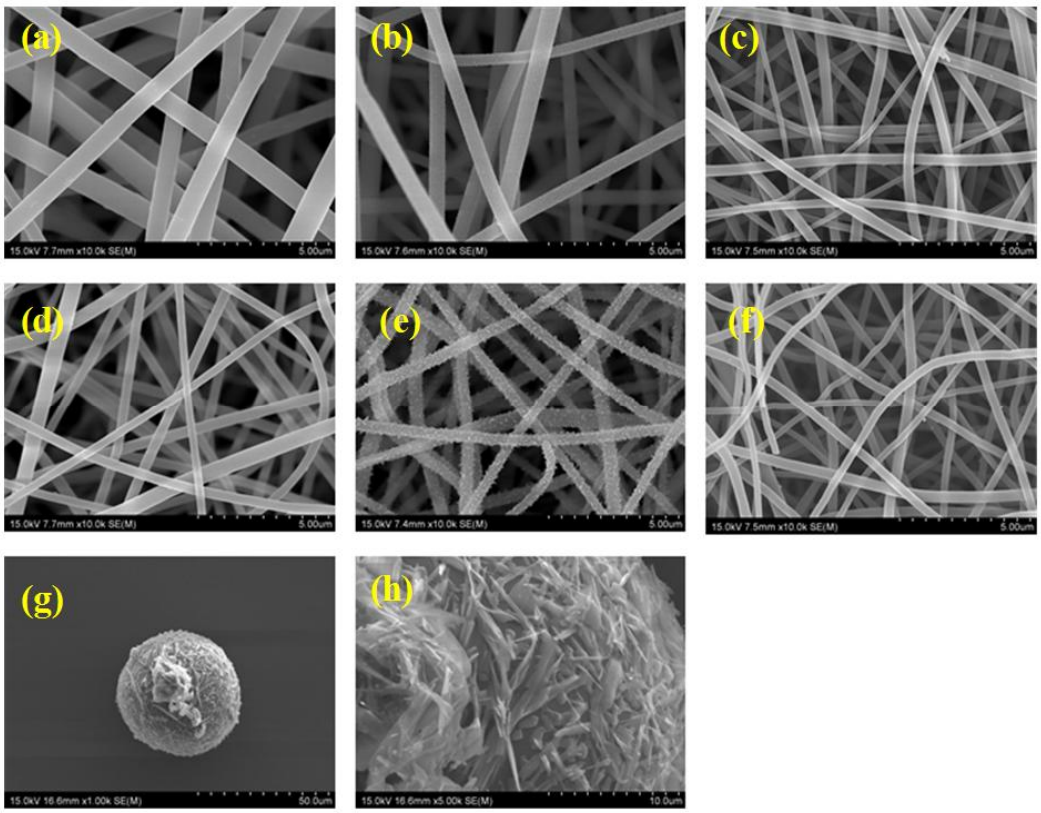

Figure 4.1. SEM images of Lig/PVA fibers with different pH (a) fiber (pH 8), (b)stabilization (pH 8), (c) carbonization (pH 8), (d) fiber (pH 9) (e) stabilization(pH 9), (f) carbonization (pH 9), (g),(h) carbonization (lignin powder)

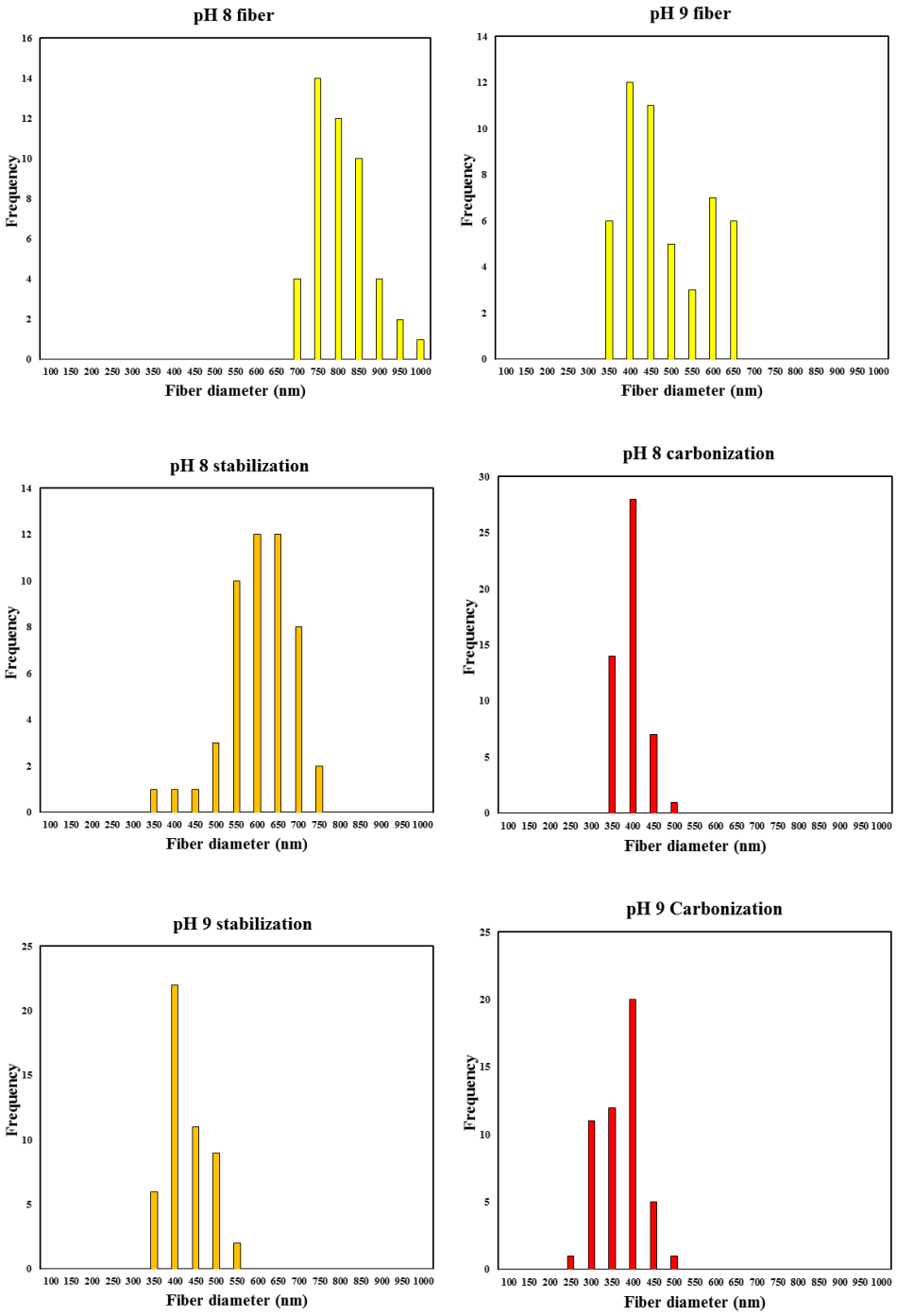

Figure 4.2. Diagram of fiber average diameter distribution through pyrolysis process

4.1.2 Fourier transform infrared (FT-IR)

The functional groups of lignin fibers were confirmed through FT-IR. As shown in Figure 4.3, the functional groups were clearly distinguished lignin fiber pH 8 and pH 9. Lignin fiber (pH 9), NaOH added fibers can be seen to retain their functionality even after stabilization and carbonization. O-H linked shearing was confirmed at 3300 cm^{-1}, and C-H symmetrical stretching was confirmed at 2885 cm^{-1}. The OH component is observed at 1630 ~ 1650 cm^{-1}. Both lignin carbon fibers (pH 8, pH 9), the stabilized fibers exhibits C-O-C asymmetrical stretching at around 1162 cm^{-1}. At 1000 cm^{-1}, C-O bond is confirmed, and lignin fiber pH 9, a glycosidic bond is observed at around 895 cm^{-1}. Based on these results, it can be confirmed that lignin carbon fibers were formed C-O-C bond in the stabilization step. Lignin fiber (pH 9) was indicated that the functional group with hydroxyl group could be confirmed,

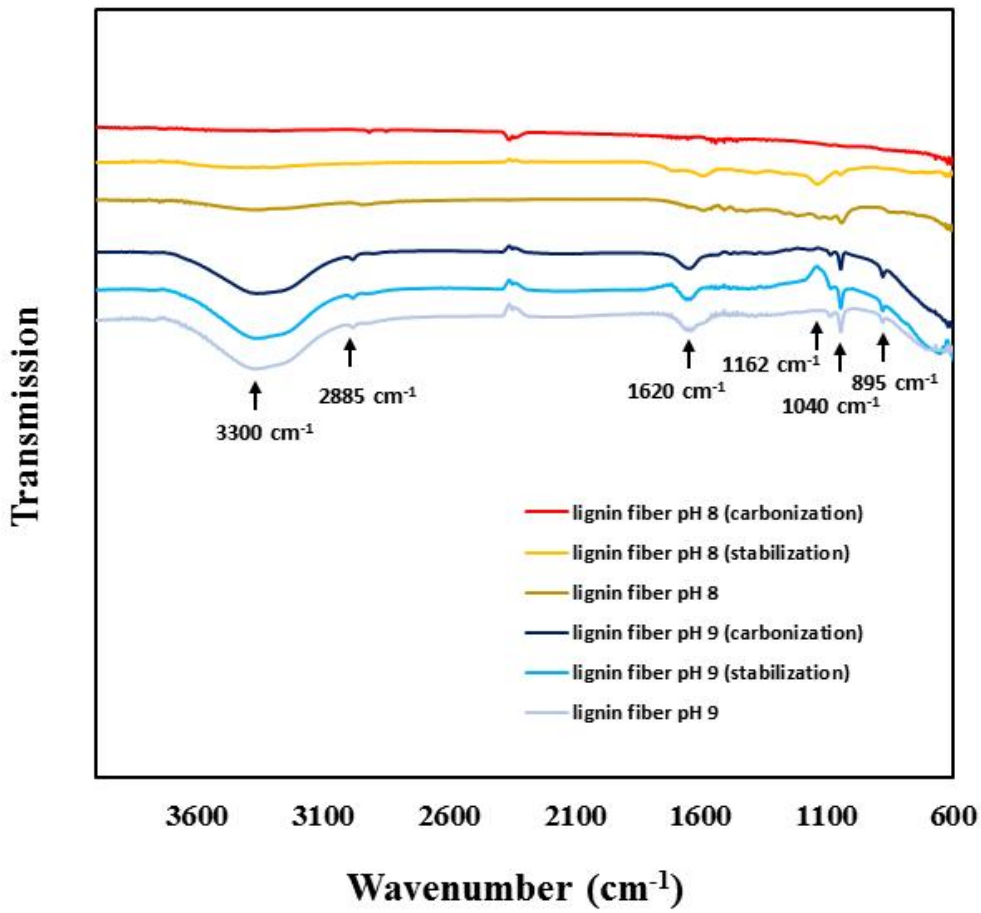

Figure 4.3. FT-IR spectra of lignin fibers pH8 and pH9 at different conditions

4.1.3 Thermogravimetric analysis (TGA)

The behaviour of polymers during heat treatment is important for making carbon fiber from kraft lignin. Thermal analysis is useful to determine whether a certain lignin is a possible precursor for carbon fiber. Stabilization and carbonization temperature, and it is possible to confirm the synthesis of PVA and lignin through reduction of thermogravimetry (Figure 4.4.). All samples, it is confirmed that the moisture is removed from the material through the rapid decrease of the heat weight in the vicinity of 100 to 300℃. The pure PVA powder is completely pyrolyzed at around 600°C and the pure lignin powder has a weight of 30% even at 900°C. The lignin fiber (pH 8) with PVA and lignin cross-linked by electrospinning had a lower thermal weight reduction than the pure PVA. In addition, the carbonization process can be smoothly achieved by keeping around 500°C without any further decrease in the thermal weight. Therefore, the stabilization condition was set at 250°C and the carbonization condition was set at 750°C. In the case of lignin fiber (pH 9) is 10% less thermogravimetric than lignin fiber (pH 8).

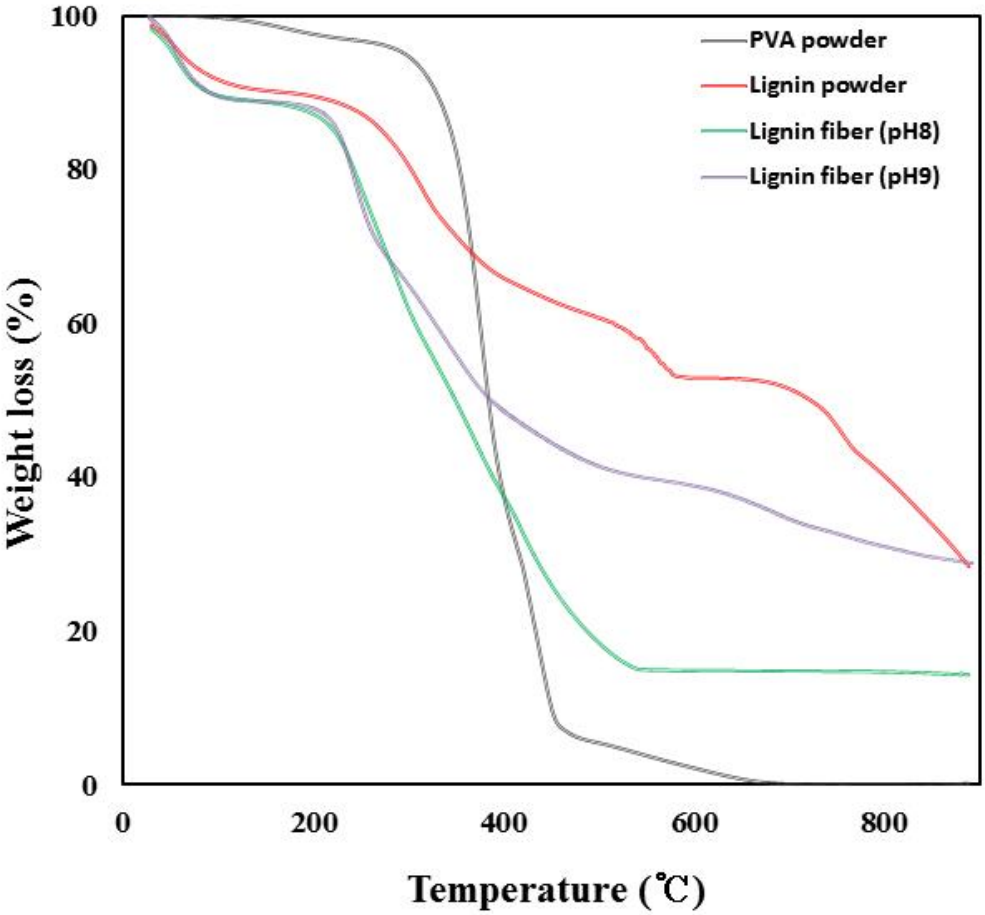

Figure 4.4. TGA thermograms of PVA/Lig fiber and precursor

4.1.4 X-ray diffraction (XRD)

When X-rays strike the crystal, some of them cause diffraction and its diffraction angle and intensity. The diffraction X-ray is used to determine the kind of the crystalline material contained in the sample and information related to the quantity. Thus, information on the structure of the crystalline material. The analytical method to be obtained is X-ray diffraction. As shown in figure 4.5, All samples showed a (002) graphite peak at around 25°, confirming that carbon crystallization was successful.

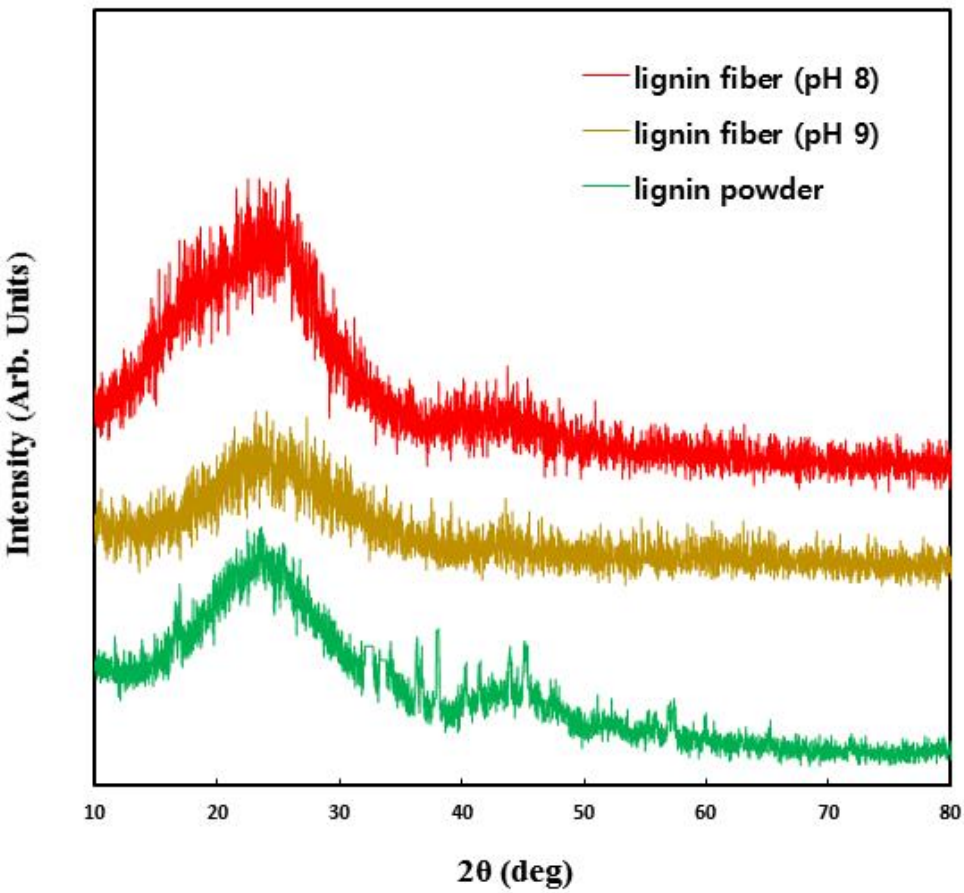

Figure 4.5. XRD patterns of lignin powder and lignin carbon fiber pH 8 and 9

4.1.5 Brunauer, emmett, teller (BET)

As shown in Figure 4.7., specific surface area of electrodes shows the adsorption / desorption isotherm for N_2 gas of activated carbon fibers and lignin powder. The adsorption isotherm results in pH 8 having 2133 m^2/g, which is twice as high as pH 9, and a specific surface area of 1099 m^2/g at pH 9. These results show that NaOH reacts only on the carbon surface, the pore block occurs, blocking the micropores of the surface and reducing the specific surface area [54,55]. However, it can be seen that the pure lignin powder has a very low specific surface area of 55 m^2/g. These results show that the fiber structure can have better adsorption characteristics than the powder form. All samples exhibit the adsorption/desorption characteristics of type-4 with hysteresis loops. The mesoporous material corresponding to hysteresis loop type-4 can be identified through the average pore size. As shown in Figure 4.6., pore size of lignin fiber (pH 8) was 2.38 nm, lignin fiber (pH 9) was 2.37 nm, and the lignin powder was 3.67 nm. These result indicated that it was a mesoporous substance.

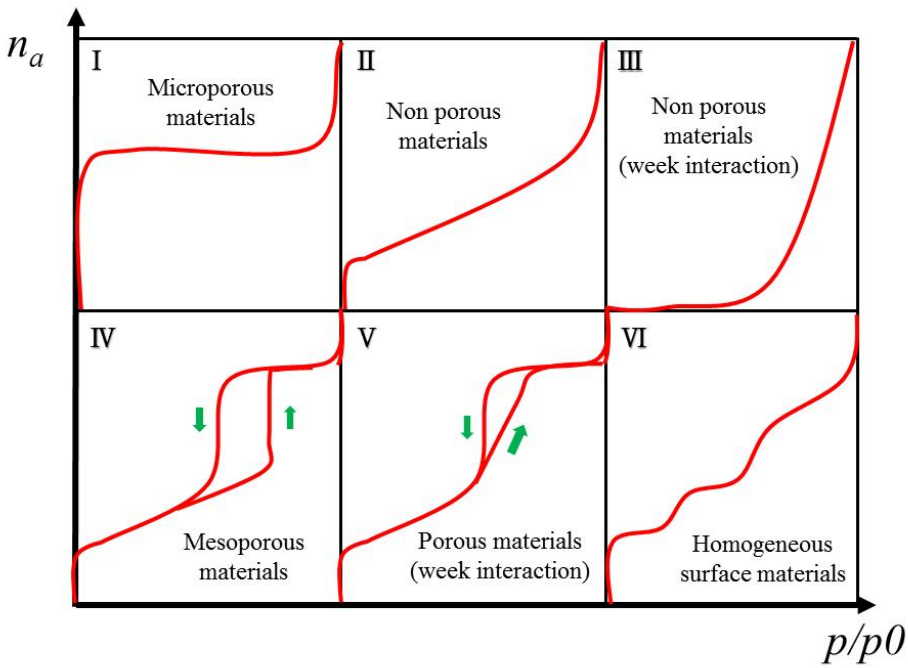

Figure 4.6. Diagrammatic Representation of Isotherm Classification

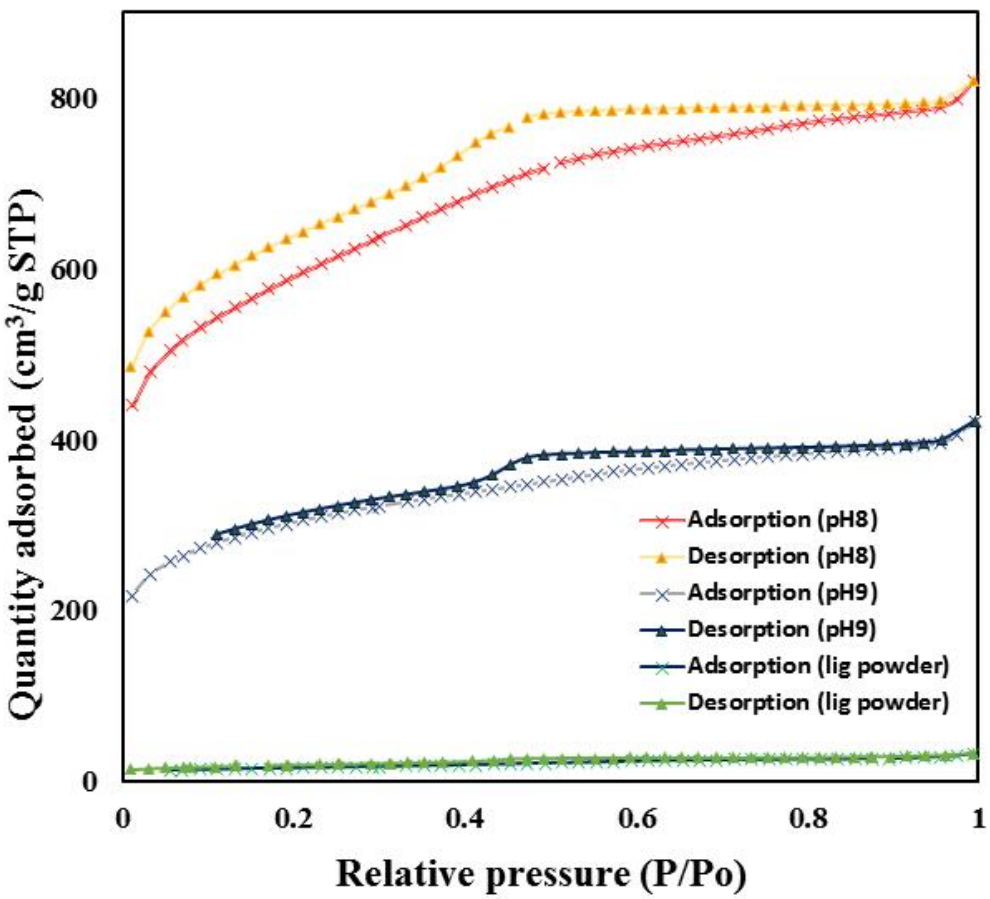

Figure 4.7. Nitrogen adsorption/desorption isotherms of lignin carbon fibers

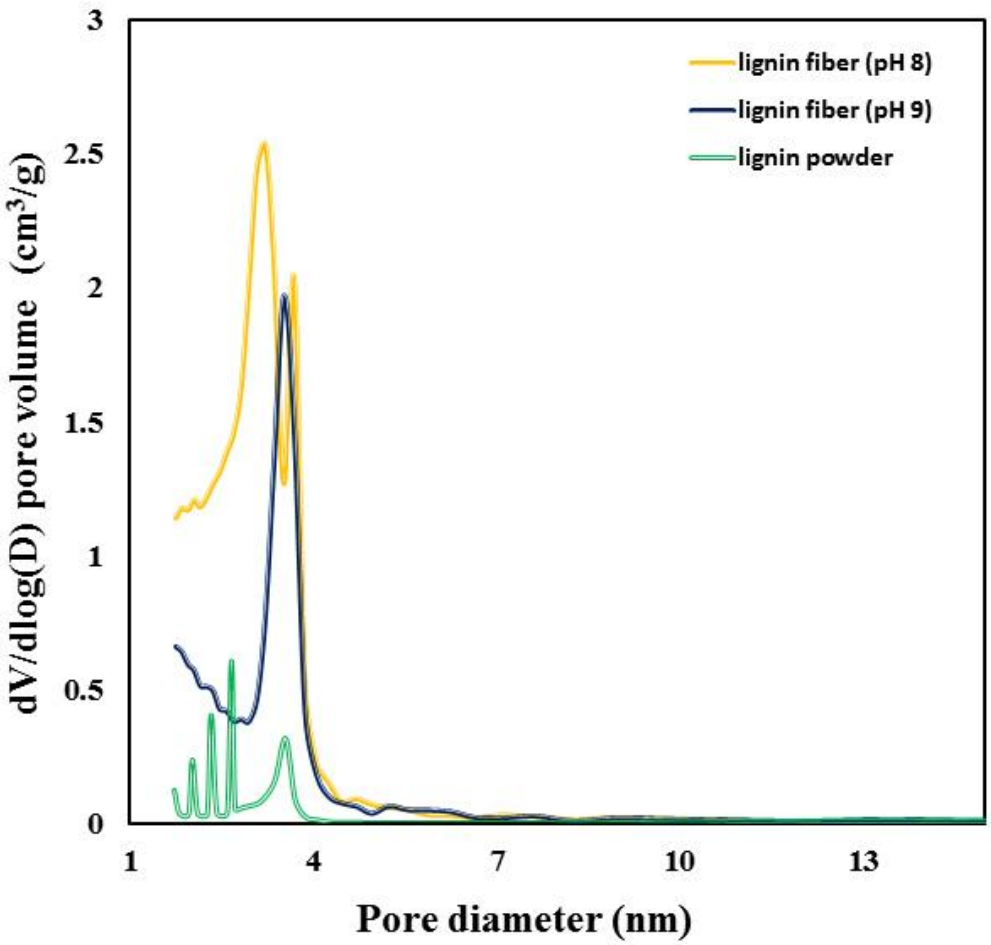

Figure 4.8. BJH pore distribution of lignin carbon fibers

Table 4.1. Values of the BET specific surface area (SSA), total pore volume, andaverage pore size acquired from N_2 adsorption isotherms at −196℃ for different carbon fibers

	BET SSA (m^2g^{-1})	Total pore Volume ($cm^3\ g^{-1}$)	Average Pore size (nm)
lignin fiber (pH 8)	2133	1.27	2.38
lignin fiber (pH 9)	1099	0.65	2.37
lignin powder	55	0.05	3.67

4.2 Electrochemical properties

4.2.1 Cyclic voltammetry (CV)

The method is used to analyze the oxidation and reduction reactions in capacitive capacitors and electrode reactions of capacitors by measuring the change of electric current with changing the potential in a certain range. In this experiment, -0.6 V ~ 0.6 V (vs. Ag / AgCl) was measured in the potential range of CV. As shown in Figure. 4.9-14, it can be seen that the current increases as the potential scanning speed increases at each activated carbon electrode. This shows that the adsorption and desorption of ions from the electrode surface is smoothly performed. When the potential scanning speed increases, the parallel concentration of the interface is changed in a state where the diffusion layer is not sufficiently grown, so that the diffusion transport occurs rapidly and the amount of generated current increases accordingly. The storage capacity is obtained by dividing the average amount of current flowing between the electrodes by the potential scanning speed (v) and the electrode weight (w).

$$\text{Capacitance (F/g)} = [(i_c + i_a)/2/v/w] \qquad \text{Equation 2}$$

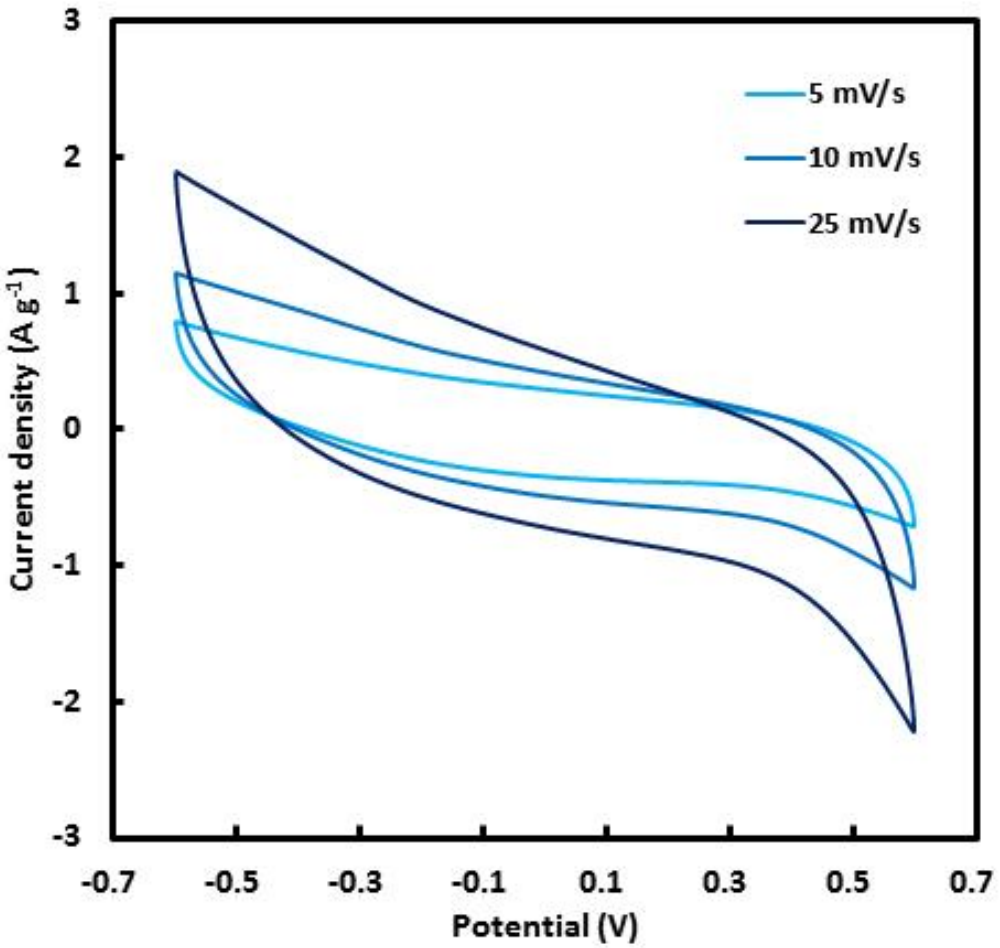

Figure 4.9. Cyclic voltammetry of lignin fiber (pH 8) electrode at 5, 10 and 25 mV/s scan rate

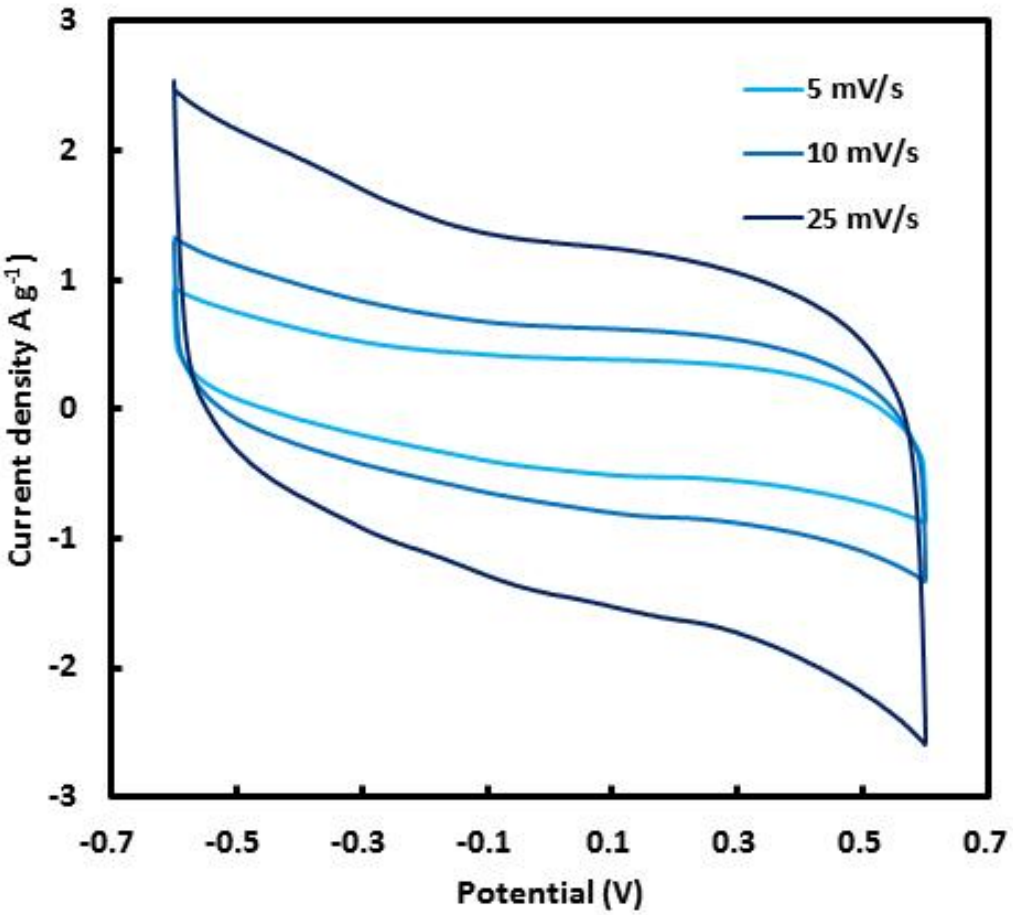

Figure 4.10. Cyclic voltammetry of lignin fiber (pH 9) electrode at 5, 10 and 25 mV/s
scan rate

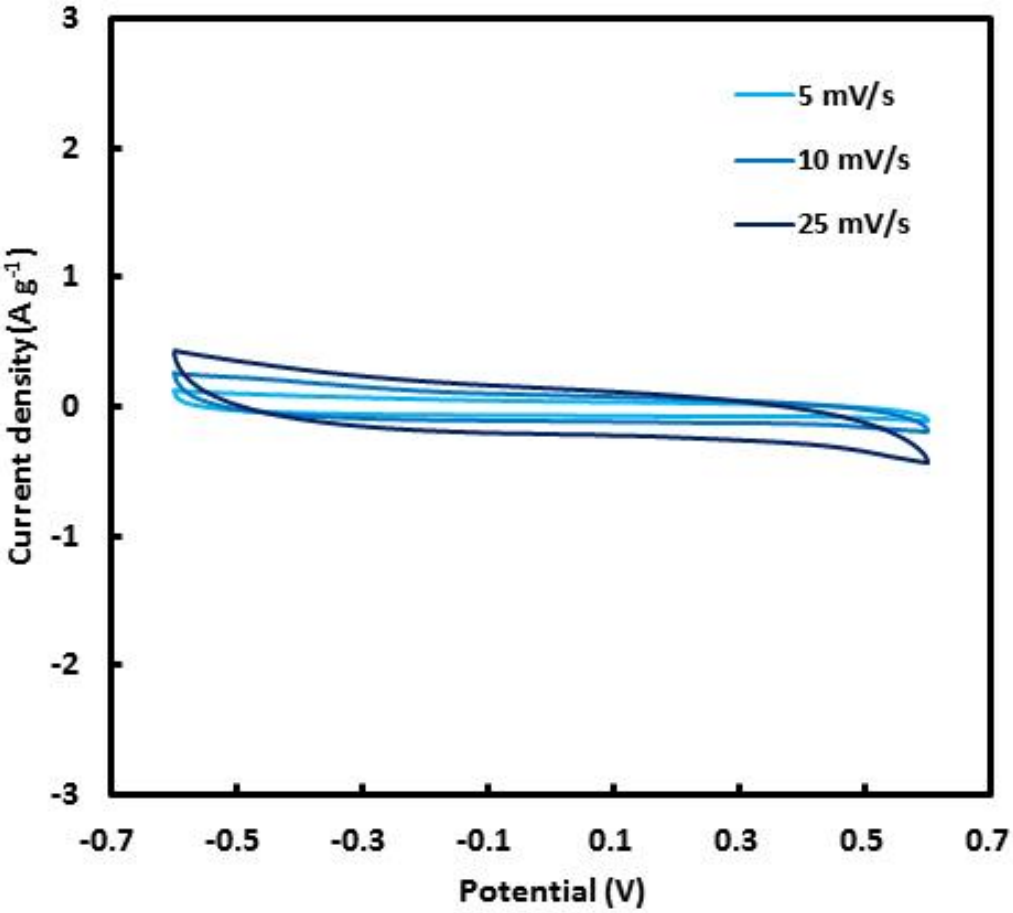

Figure 4.11 Cyclic voltammetry of lignin powder electrode at 5, 10 and 25 mV/s scan rate

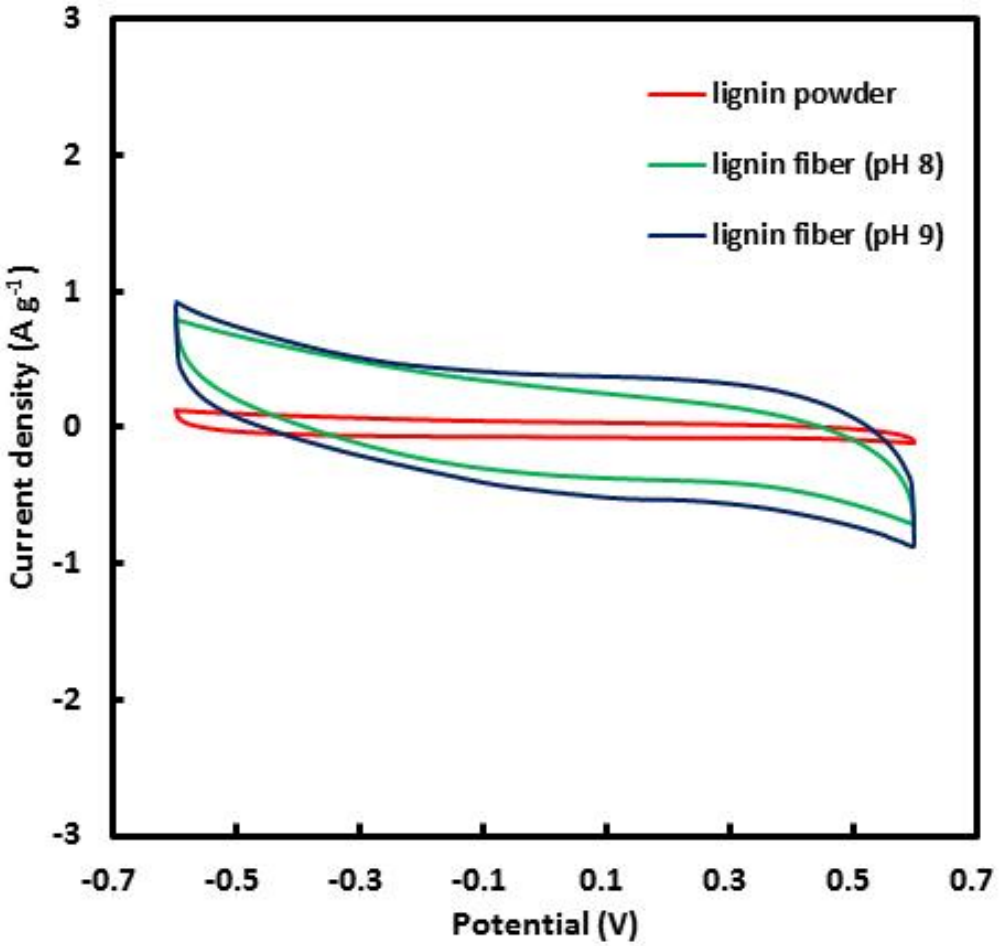

Figure 4.12. Cyclic voltammetry of 3 electrodes at 5 mV/s scan rate

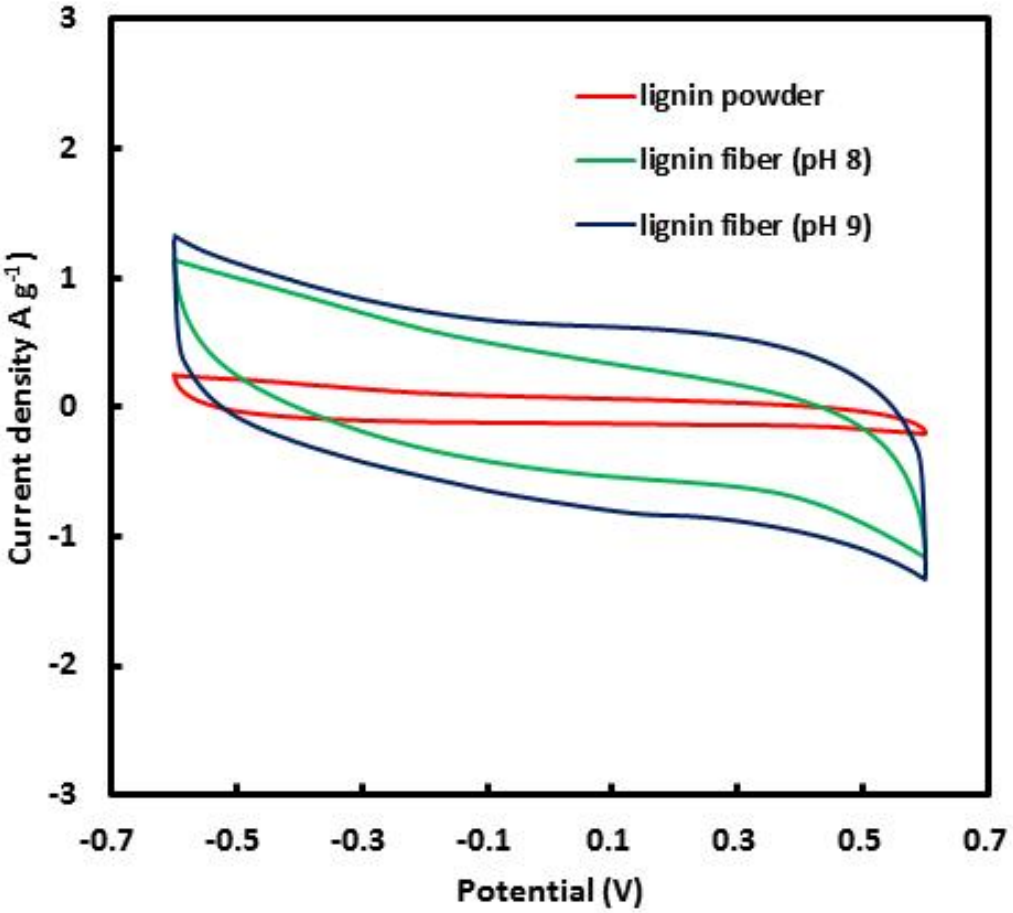

Figure 4.13. Cyclic voltammetry of 3 electrodes at 10 mV/s scan rate

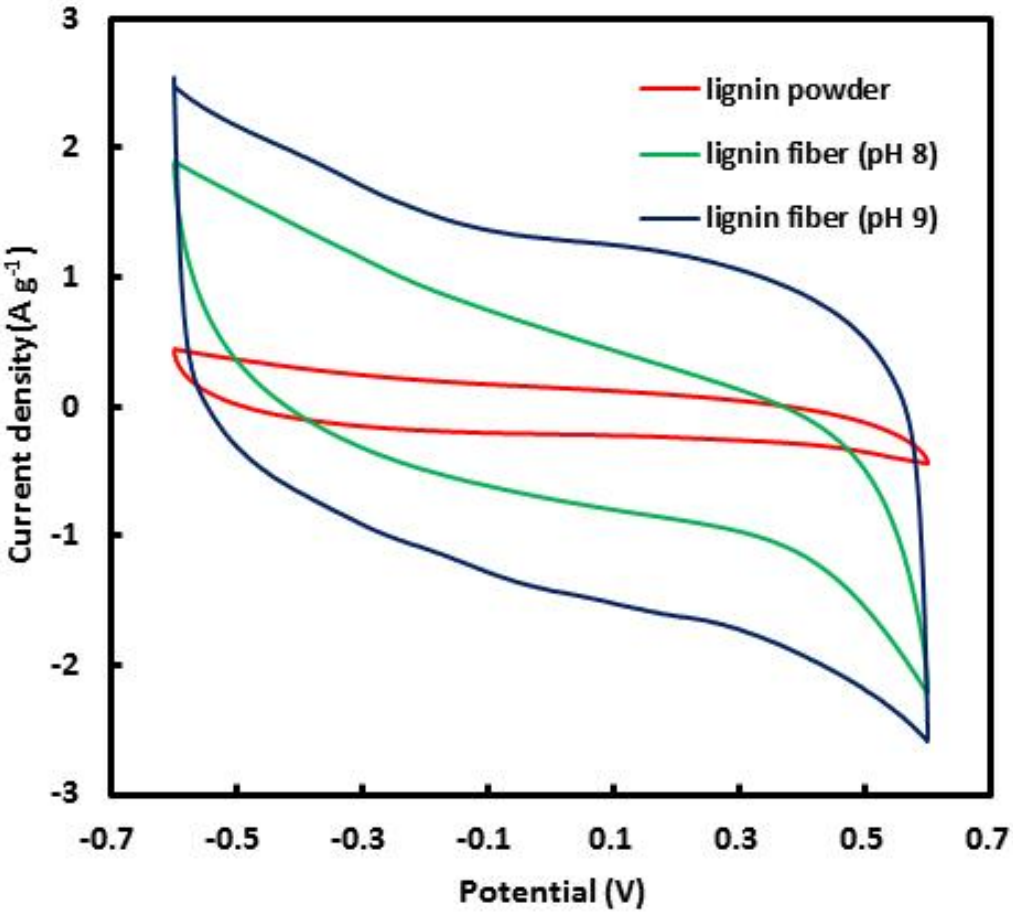

Figure 4.14. Cyclic voltammetry of 3 electrodes at 25 mV/s scan rate

Table 4.2. Capacitances of carbon electrodes at 5.0, 10.0 and 25.0 mV/s scan rate

Scan rate (mV/s)	Capacitance (F/g)		
	lignin fiber (pH 8)	lignin fiber (pH 9)	lignin powder
5	117	143	19
10	83	114	17
25	47	90	16

4.2.2 AC impedance

The electric double layer at the interface between electrode and electrolyte is equivalent to a circuit in which the electric capacity and the electric resistance were connected in series. Therefore, the electrical characteristics of the electrode interface can be effectively observed through the impedance analysis. Impedance was measured at 0 V while varying the frequency from 0.01 Hz to 100,000 Hz. As a result, Figure .4.15 shows the equivalent circuit for material transport. Table 4.3 shows the interfacial resistance and solution resistance of each electrode. Figure .4.16 shows the nyquist plot for each carbon electrode. Table 4.4 shows the solution resistance and interfacial resistance of each carbon electrode. The resistance at the interface was lowest at pH 8, then at pH 9 and then at lignin powder was low. The nyquist plot can be used to check the shape of the carbon structure. In Figure 4.17., we could expected that lignin fibers (pH 8 and 9) had a pore shape close similar to the cylinder. The lignin powder form has a pore shape similar to the bubble.

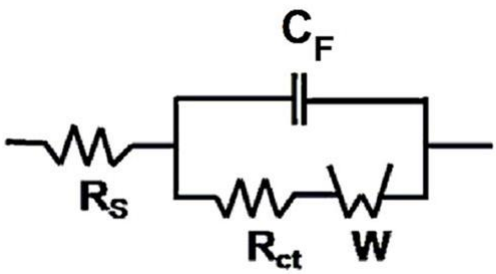

Figure 4.15. The equivalent circuit of lignin carbon fibers

Table 4.3. The polarization resistance and charge transfer resistance of carbon electrodes

	R_s (Ω)	R_{ct} (Ω)
lignin fiber (pH 8)	6.782	0.363
lignin fiber (pH 9)	4.079	0.431
lignin powder	1.806	0.649

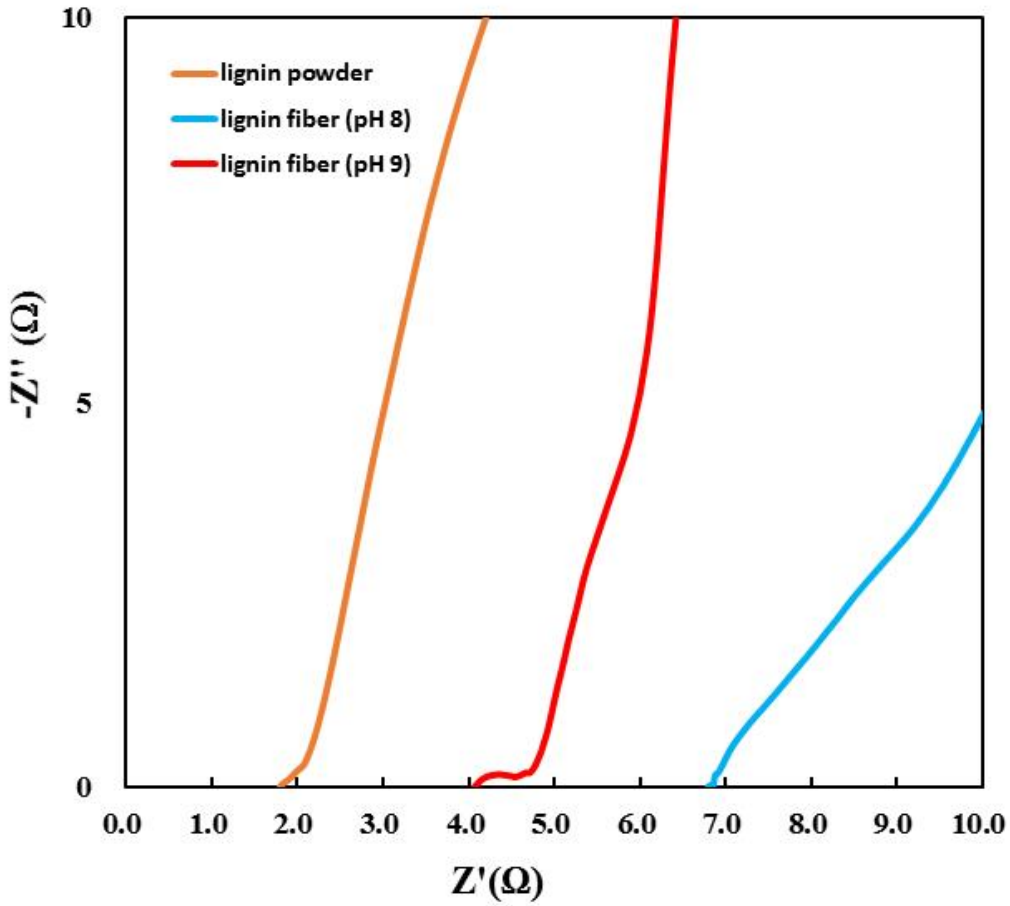

Figure 4.16. Nyquist plot for lignin carbon fiber electrodes prepared with pH 8, pH 9 and lignin powder

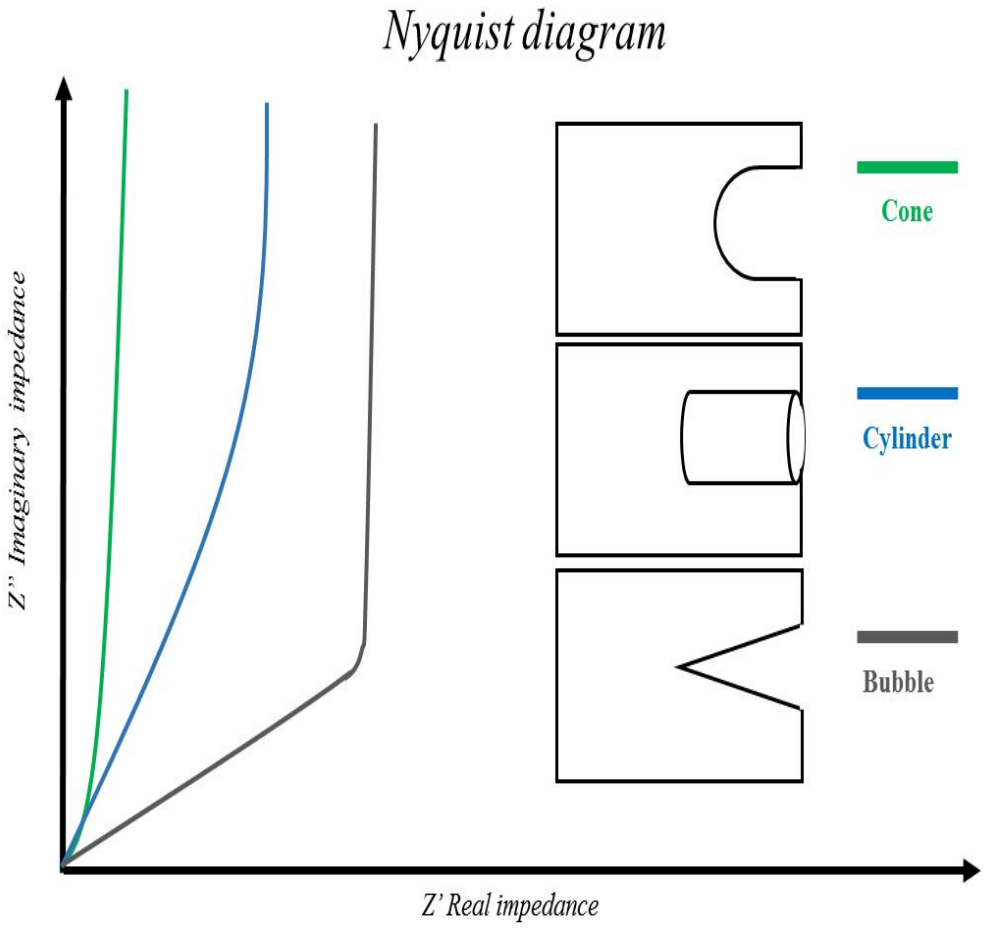

Figure 4.17. The shape of pores according to electro impedance [56].

4.2.3 Chronoamperometry & chronocoulometry

CA was used to observe the characteristics of adsorption and desorption of carbon electrodes by measuring the current change with time while applying a constant potential. The adsorption characteristics of ions were confirmed by changing the current with time while applying a constant electrode potential of -0.6 V (vs. Ag / AgCl) to the carbon electrode for 200 sec. As shown in Figure. 4.18, it can be seen that lignin fiber (pH 9) has a current value higher than lignin fiber (pH 8). These results show that the NaOH chemical activation method can improve electrical performance, which is similar in chronocoulometry. CC is a method of measuring the change of the ceharge amount with time while applying a constant electric potential and shows the amount of electric charge flowing in the adsorption and desorption process. Since the electric adsorption takes place at a potential at which no electrode reaction occurs at the electrode surface, the amount of current flowing through the electrode is proportional to the amount of ions adsorbed on the electrode surface. As shown in Figure. 4.19, it can be seen that lignin fiber (pH 9) has a higher capacity than lignin fiber (pH 8).

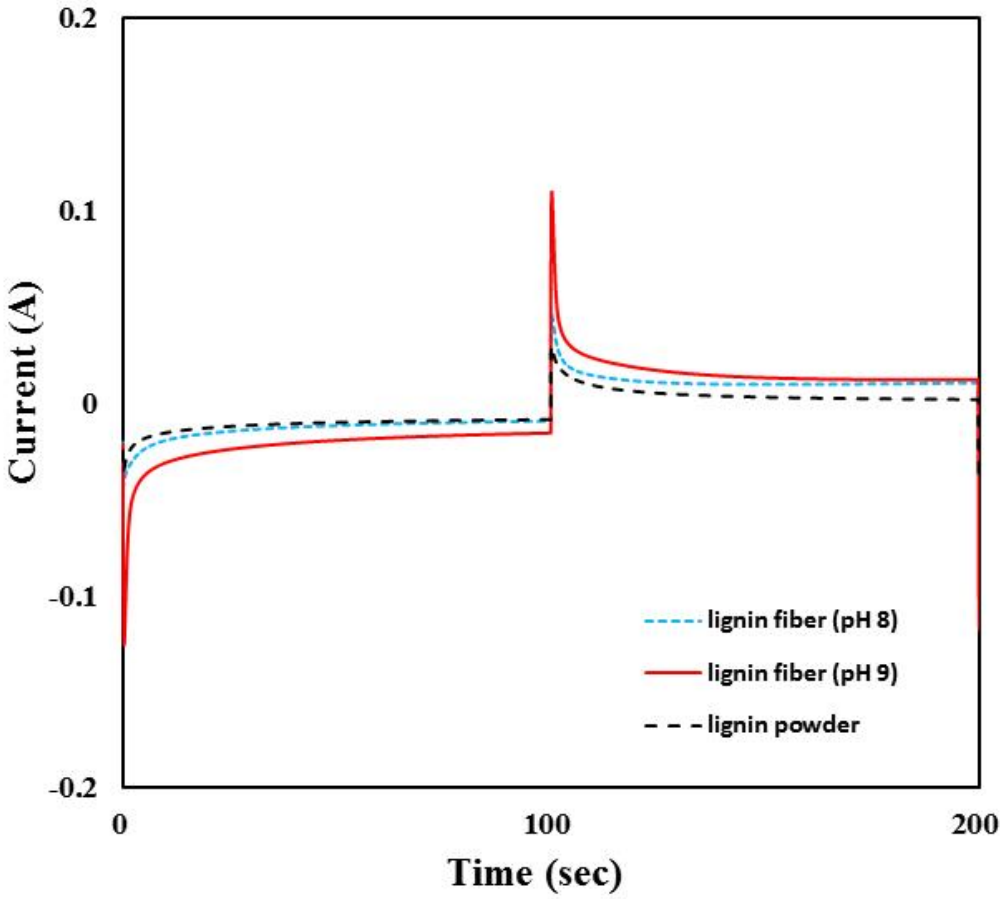

Figure 4.18. Change in current density with time at the constant potential of −0.6 and 0.6 V vs. Ag/AgCl

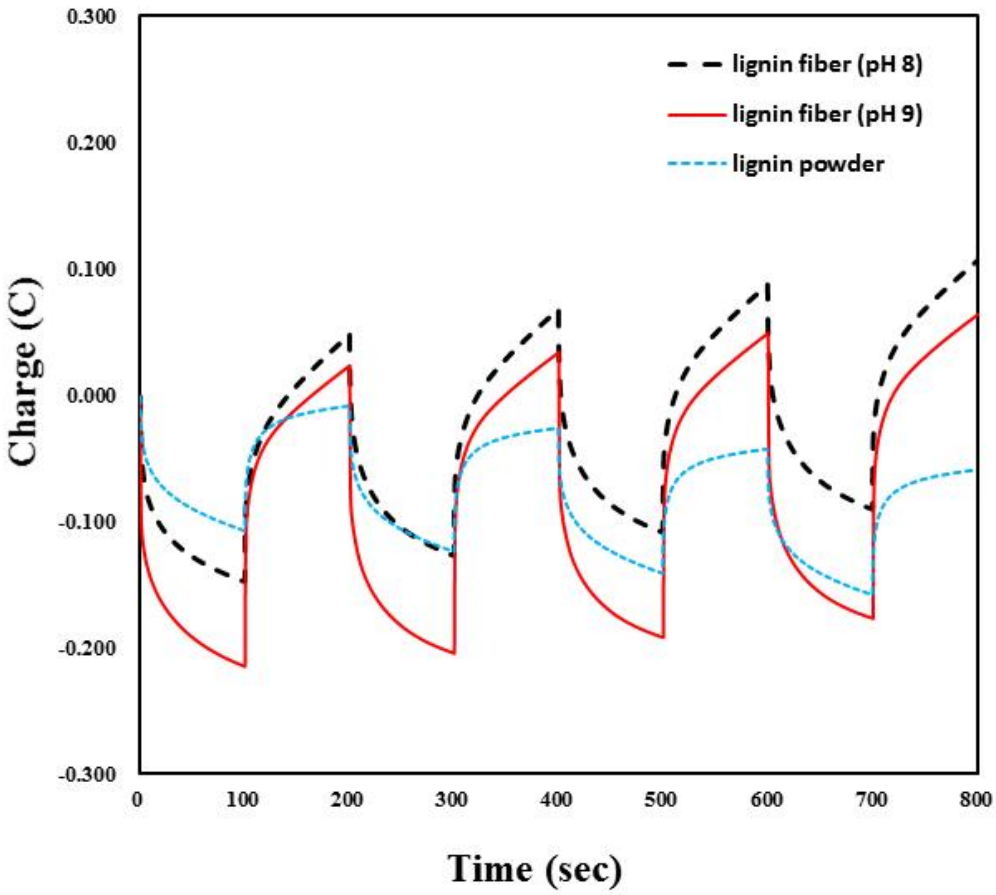

Figure 4.19. Change in cumulative charges with time at the constant potential of −0.6 and 0.6 V vs. Ag/AgCl

4.3 Desalination performance of CDI

The desalination efficiency of each carbon electrodes was measured. Experiment was carried out with a potential of 1.2 V while flowing a 100 mg/L NaCl aqueous solution at 15 ml/min using lignin fibers (pH 8 and 9) and lignin powder. The results of the conductivity measured in the adsorption /desorption reaction three electrodes are shown in Figure. 4.20. When the potential was applied, the electrical conductivity was rapidly monitored during the adsorption process and gradually increased after about 3 min. Lignin fiber (pH 9) showed the lowest conductivity, followed by lignin fiber (pH 8), and lignin powder. The efficiency of desalination was 63.5% for lignin powder, 77.2% for lignin fiber (pH 8) and 85.4% for lignin fiber (pH 9).

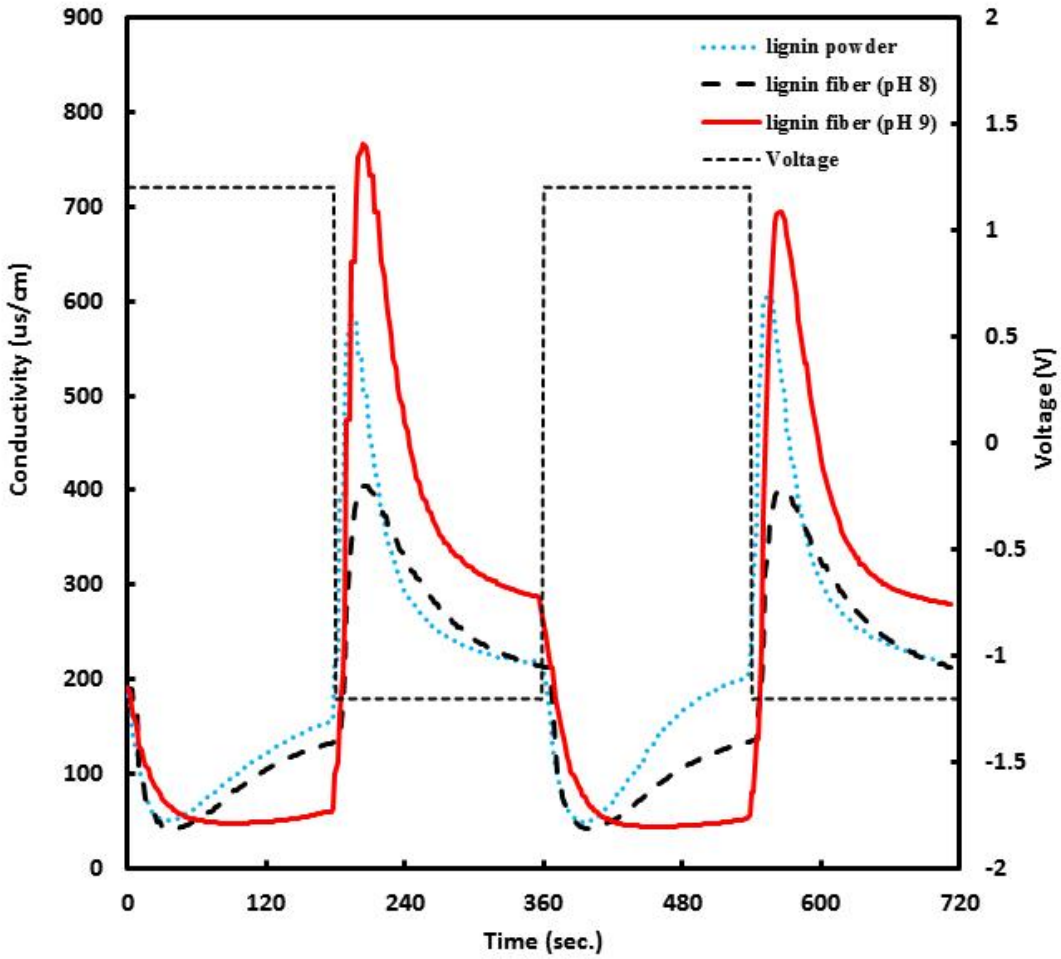

Figure 4.20. Desalination performance of various carbon electrodes

Chapter 5. Conclusion

The lignin carbon fibers were successfully prepared by electrospinning method using pure lignin and PVA mixture solution. It was found from FE-SEM that the fiber diameter distribution of the carbon fibers was highly uniform. From the analysis of BET measurement of lignin carbon fibers, the specific surface area of lignin fibers (pH 8 and 9) were 2133 m^2/g and 1099 m^2/g, respectively. In addition, the carbon fiber obtained under pH 8 showed the higher surface area with well-developed micro pores. However, the carbon fiber obtained under pH 9 was relatively lower surface area with mesopores. The capacitance of the carbon fibers were measured by cyclic voltammetry using a small electrode. The capacitances for lignin fibers (pH 8, 9) were 117 F/g and 143 F/g, respectively. The lignin carbon fibers were applied as a carbon electrode for CDI. As a result, the desalination efficiencies were 77.2% for pH 8 and 85.4% for pH 9 under the experimental conditions of 100 mg/L of sodium chloride and 1.2 V of applied voltage. For the practical application of the actual lignin black liquor solution, similar studies will be continued for the preparation, characterization and application of the electrospun lignin carbon fibers from lignin black liquor.

References

[1] Hansen, J.; Ruedy, R.; Sato, M.; Lo, K., Global surface temperature change. *Reviews of Geophysics* **2010,** *48* (4).

[2] Fischer, E. M.; Knutti, R., Anthropogenic contribution to global occurrence of heavy-precipitation and high-temperature extremes. *Nature Climate Change* **2015,** *5* (6), 560-564.

[3] Kummu, M.; Ward, P. J.; de Moel, H.; Varis, O., Is physical water scarcity a new phenomenon? Global assessment of water shortage over the last two millennia. *Environmental Research Letters* **2010,** *5* (3), 034006.

[4] Vörösmarty, C. J.; Green, P.; Salisbury, J.; Lammers, R. B., Global water resources: vulnerability from climate change and population growth. *science* **2000,** *289* (5477), 284-288.

[5] Kim, Y.; Chung, E.-S.; Jun, S.-M., Iterative framework for robust reclaimed wastewater allocation in a changing environment using multi-criteria decision making. *Water resources management* **2015,** *29* (2), 295-311.

[6] Thu, K. Adsorption desalination: theory & experiments. **2010**

[7] IDA Young Leaders Program **2014.**

[8] Khawaji, A. D.; Kutubkhanah, I. K.; Wie, J.-M., Advances in seawater desalination technologies. Desalination **2008**, 221 (1), 47-69.

[9] Al-Mutaz, I. S.; Wazeer, I., Comparative performance evaluation of conventional multi-effect evaporation desalination processes. Applied Thermal Engineering **2014**, 73 (1), 1194-1203.

[10] Ortega-Delgado, B.; Cornali, M.; Palenzuela, P.; Alarcón-Padilla, D. C., Operational analysis of the coupling between a multi-effect distillation unit with thermal vapor compression and a Rankine cycle power block using variable nozzle thermocompressors. Applied Energy **2017**, 204 (Supplement C), 690-701.

[11] Fritzmann, C.; Löwenberg, J.; Wintgens, T.; Melin, T., State-of-the-art of reverse osmosis desalination. Desalination **2007**, 216 (1), 1-76.

[12] Jamaly, S.; Darwish, N. N.; Ahmed, I.; Hasan, S. W., A short review on reverse osmosis pretreatment technologies. Desalination **2014**, 354 (Supplement C), 30-38.

[13] Shenvi, S. S.; Isloor, A. M.; Ismail, A. F., A review on RO membrane technology: Developments and challenges. Desalination **2015**, 368 (Supplement C), 10-26.

[14] Wijmans, J. G.; Baker, R. W., The solution-diffusion model: a review. Journal of Membrane Science **1995**, 107 (1), 1-21.

[15] Soltanieh, M.; Gill, W. N., REVIEW OF REVERSE OSMOSIS MEMBRANES AND TRANSPORT MODELS. Chemical Engineering Communications **1981**, 12 (4-6), 279-363.

[16] Huang, C.; Xu, T.; Zhang, Y.; Xue, Y.; Chen, G., Application of electrodialysis to the production of organic acids: State-of-the-art and recent developments. Journal of Membrane Science **2007**, 288 (1), 1-12.

[17] Saracco, G., Ionic membrane technologies for the recovery of valuable chemicals from waste waters. Ann Chim **2003**, 93 (9-10), 817-826.

[18] Xu, T.; Huang, C., Electrodialysis-based separation technologies: A critical review. AIChE Journal **2008**, 54 (12), 3147-3159.

[19] Manecke, G., Ionenaustauscher, Band I: Grundlagen. Struktur - Herstellung – Theorie, von F. Helfferich. Verlag Chemie GmbH., Weinheim/Bergstraße 1959. 1. Aufl., VIII, 520 S., 153 Abb., 14 Tab., geb. DM 48.–. Angewandte Chemie **1962**, 74 (15), 596-596.

[20] Greiter, M.; Novalin, S.; Wendland, M.; Kulbe, K.-D.; Fischer, J., Desalination of whey by electrodialysis and ion exchange resins: analysis of both processes with regard to sustainability by calculating their cumulative energy demand. Journal of Membrane Science **2002**, 210 (1), 91-102.

[21] 2014AXEON Water Technologies **2014.**

[22] Porada, S.; Zhao, R.; van der Wal, A.; Presser, V.; Biesheuvel, P. M., Review on the science and technology of water desalination by capacitive deionization. Progress in Materials Science **2013**, 58 (8), 1388-1442.

[23] Johnson, A. M.; Newman, J., Desalting by Means of Porous Carbon Electrodes. Journal of The Electrochemical Society **1971**, 118 (3), 510-517.

[24] Johnson, A.; Venolia, A.; Newman, J.; Wilbourne, R.; Wong, C.; Gillam, W.; Johnson, S.; Horowitz, R., Electrosorb process for desalting water, Office of Saline Water Research and Development. In Progress Report No 516, US Department of the Interior, Publication 200 056, **1970**.

[25] Sharma, P.; Bhatti, T., A review on electrochemical double-layer capacitors. Energy conversion and management **2010**, 51 (12), 2901-2912.

[26] Jia, B.; Zhang, W., Preparation and Application of Electrodes in Capacitive Deionization (CDI): a State-of-Art Review. Nanoscale research letters **2016**, 11 (1), 64.

[27] Garcia-Quismondo, E.; Gomez, R.; Vaquero, F.; Cudero, A. L.; Palma, J.; Anderson, M., New testing procedures of a capacitive deionization reactor. *Physical Chemistry Chemical.*

[28] Thamilselvan, A.; Nesaraj, A.; Noel, M., Review on carbon-based electrode materials for application in capacitive deionization process. *International Journal of Environmental Science and Technology* **2016,** *13* (12), 2961-2976.

[29] Helmholtz, H. V., Studien über electrische Grenzschichten. Annalen der Physik **1879**, 243 (7), 337-382.

[30] Masliyah, J. H.; Bhattacharjee, S., Electrokinetic and colloid transport phenomena. John Wiley & Sons: **2006.**

[31] Bagotsky, V., Nonaqueous electrolytes. Fundamentals of Electrochemistry, Second Edition **2006,** 127-137.

[32] Bard, A. J.; Faulkner, L. R., Fundamentals and applications. Electrochemical Methods **2001**, 2.

[33] Gouy, M., Sur la constitution de la charge électrique à la surface d'un électrolyte. J. Phys. Theor. Appl. **1910**, 9 (1), 457-468.

[34] Chapman, D. L., LI. A contribution to the theory of electrocapillarity. The London, Edinburgh, and Dublin philosophical magazine and journal of science **1913**, 25 (148), 475-481.

[35] Zhang, L. L.; Zhao, X., Carbon-based materials as supercapacitor electrodes. Chemical Society Reviews **2009**, 38 (9), 2520-2531.

[36] Stern, O., Zur theorie der elektrolytischen doppelschicht. Berichte der Bunsengesellschaft für physikalische Chemie **1924**, 30 (21-22), 508-516.

[37] Conway, B., Electrochemical Supercapacitors: Sci-entific Fundamentals and Technological Applications. Kluwer-Plenum. **1999.**

[38] Grahame, D. C., The electrical double layer and the theory of electrocapillarity. Chemical reviews **1947**, 41 (3), 441-501.

[39] Pilon, L.; Wang, H.; d'Entremont, A., *Recent Advances in Continuum Modeling of Interfacial and Transport Phenomena in Electric Double Layer Capacitors*. 2015; Vol. 162, p A5158-A5178.

[40] Kim, Y.-J.; Choi, J.-H., Enhanced desalination efficiency in capacitive deionization with an ion-selective membrane. **2010**; Vol. 71, p 70-75.

[41] Wang, G.; Qian, B.; Dong, Q.; Yang, J.; Zhao, Z.; Qiu, J., Highly mesoporous activated carbon electrode for capacitive deionization. Separation and Purification Technology **2013**, 103 (Supplement C), 216-221.

[42] Lu, H., Biomass-derived carbon electrode materials for supercapacitors. *Sustainable Energy & Fuels* **2017**.

[43] Jeon, S.-i.; Park, H.-r.; Yeo, J.-g.; Yang, S.; Cho, C. H.; Han, M. H.; Kim, D. K., Desalination via a new membrane capacitive deionization process utilizing flow-electrodes. *Energy & Environmental Science* **2013,** *6* (5), 1471-1475.

[44] Porada, S.; Weingarth, D.; Hamelers, H.; Bryjak, M.; Presser, V.; Biesheuvel, P., Carbon flow electrodes for continuous operation of capacitive deionization and capacitive mixing energy generation. *Journal of Materials Chemistry A* **2014,** *2* (24), 9313-9321.

[45] Gendel, Y.; Rommerskirchen, A. K. E.; David, O.; Wessling, M., Batch mode and continuous desalination of water using flowing carbon deionization (FCDI) technology. *Electrochemistry Communications* **2014,** *46*, 152-156.

[46] Wang, H.; Zhang, D.; Yan, T.; Wen, X.; Zhang, J.; Shi, L.; Zhong, Q., Three-dimensional macroporous graphene architectures as high performance electrodes for capacitive deionization. *Journal of Materials Chemistry A* **2013,** *1* (38), 11778-11789.

[47] Yang, Z. Y.; Jin, L. J.; Lu, G. Q.; Xiao, Q. Q.; Zhang, Y. X.; Jing, L.; Zhang, X. X.; Yan, Y. M.; Sun, K. N., Sponge-templated preparation of high surface area graphene with ultrahigh capacitive deionization performance. *Advanced Functional Materials* **2014,** *24* (25), 3917-3925.

[48] Wang, H.; Yan, T.; Liu, P.; Chen, G.; Shi, L.; Zhang, J.; Zhong, Q.; Zhang, D., In situ creating interconnected pores across 3D graphene architectures and their application as high performance electrodes for flow-through deionization capacitors. *Journal of Materials Chemistry A* **2016,** *4* (13), 4908-4919.

[49] Belessiotis, V.; Delyannis, E., Water shortage and renewable energies (RE) desalination possible technological applications. Desalination **2001**, 139 (1), 133-138.

[50] Ago, M.; Jakes, J. E.; Johansson, L.-S.; Park, S.; Rojas, O. J., Interfacial properties of lignin-based electrospun nanofibers and films reinforced with cellulose nanocrystals. *ACS*

applied materials & interfaces **2012,** *4* (12), 6849-6856.

[51] Ago, M.; Okajima, K.; Jakes, J. E.; Park, S.; Rojas, O. J., Lignin-based electrospun nanofibers reinforced with cellulose nanocrystals. *Biomacromolecules* **2012,** *13* (3), 918-926.

[52] Yusof, N.; Ismail, A., Post spinning and pyrolysis processes of polyacrylonitrile (PAN)-based carbon fiber and activated carbon fiber: A review. *Journal of Analytical and Applied Pyrolysis* **2012,** *93*, 1-13.

[53] Son, W. K.; Youk, J. H.; Lee, T. S.; Park, W. H., Effect of pH on electrospinning of poly (vinyl alcohol). *Materials letters* **2005,** *59* (12), 1571-1575.

[54] Shim, J.-W.; Park, S.-J.; Ryu, S.-K., Effect of modification with HNO 3 and NaOH on metal adsorption by pitch-based activated carbon fibers. *Carbon* **2001,** *39* (11), 1635-1642.

[55] Hu, S.; Zhang, S.; Pan, N.; Hsieh, Y.-L., High energy density supercapacitors from lignin derived submicron activated carbon fibers in aqueous electrolytes. *Journal of Power Sources* **2014,** *270*, 106-112.

[56] Mariani, A.; Thanapalan, K.; Stevenson, P.; Williams, J., An advanced prediction mechanism to analyse pore geometry shapes and identification of blocking effect in VRLA battery system. *International Journal of Automation and Computing* **2017,** *14* (1), 21-32.